Fluid Phase Equilibria 511 (2020) 112498

Contents lists available at ScienceDirect

Fluid Phase Equilibria

journal homepage: www.elsevier.com/locate/fluid

Hydrogen sulfide solubility in 50 wt% and 70 wt% aqueous methyldiethanolamine at temperatures from 283 to 393 K and total pressures from 500 to 10000 kPa

Eirini Skylogianni [a], Ingvild Mundal [a], Diego D.D. Pinto [a], Christophe Coquelet [b], Hanna K. Knuutila [a, *]

[a] Department of Chemical Engineering, Norwegian University of Science and Technology, Sem Sælands vei 6, 7034, Trondheim, Norway
[b] Mines ParisTech - PSL University, CTP- Centre of Thermodynamics of Processes, 35 rue Saint Honoré, 77305, Fontainebleau, France

ARTICLE INFO

Article history:
Received 26 November 2019
Received in revised form
22 January 2020
Accepted 23 January 2020
Available online 29 January 2020

Keywords:
Gas processing
Absorption
Hydrogen sulfide
Methane
MDEA
High pressure
Vapor-liquid equilibrium
Vapor pressure

ABSTRACT

The hydrogen sulfide (H_2S) absorption capacity of a 70 wt% aqueous methyldiethanolamine (MDEA) solution was investigated in a static-analytic apparatus at temperatures of 283, 353 and 393 K and pressures of 2000, 6000 and 10000 kPa in the presence of methane. New experimental data were also produced for a 50.1 wt% aqueous MDEA at 323 K and pressures of 500 and 3000 kPa as part of the apparatus validation procedure. A model based on electrolyte non-random two-liquid (eNRTL) activity coefficient model to describe the liquid phase and Peng-Robinson Equation of State to describe the vapor phase non-idealities was developed for the system H_2S-MDEA-H_2O, which can potentially be used also for the system in the presence of methane at low pressures. Vapor pressure measurements of pure MDEA were also performed in the range of 405–435 K in an ebulliometer and parameters for the Antoine correlation were proposed.

1. Introduction

Natural and refinery gas streams usually contain acid gases, carbon dioxide and sulfur compounds, which must be removed in order to ensure trouble-free and safe operations. Typical sulfur compounds are hydrogen sulfide, carbonyl sulfide, mercaptans, with the first one being the most important one as it occurs in the largest concentrations [1]. Hydrogen sulfide (H_2S) gas content is routinely controlled by absorption into aqueous methyldiethanolamine (MDEA), which can then be thermally regenerated and reused.

A 50 wt% MDEA-H_2O concentration is considered a benchmark solvent in H_2S removal, due to its equilibrium behavior and low corrosion. Aqueous MDEA has been long established in the industry due to among others, the amine's availability, low cost and energy requirements, resistance to degradation, ability to meet the 4 ppm specification requirement for pipeline gas and to selectively remove H_2S over CO_2, which often coexist. MDEA owes its latter characteristic to its structure; as a tertiary amine, aqueous MDEA reacts instantaneously with hydrogen sulfide while it requires more time to react with CO_2. Thus, by regulating the contact time between the solvent and the gas, H_2S removal to specification and minimum co-absorption of CO_2 can be achieved [2,3].

The motivation of this work has been the investigation of highly concentrated MDEA for the combined H_2S removal and hydrate control for subsea application. Oil and gas reservoirs are turning sour in the course of time [4,5], which is tackled today by using triazine to control the H_2S levels [6]. Main disadvantages of employment of triazine are related to the non-regeneration of the solvent, weight, space, transportation and disposal requirements. These constraints are of outmost importance, especially as the available production fields are sourer, deeper and in longer distances from the shore [7]. MDEA is already used offshore as a pH stabilizer [8] facilitating its employment subsea, while the fact that, as a polar

* Corresponding author.
E-mail address: hanna.knuutila@ntnu.no (H.K. Knuutila).

https://doi.org/10.1016/j.fluid.2020.112498

compound, it has affinity for water, renders highly concentrated aqueous MDEA a good candidate for acting both as a hydrate inhibitor and as an H_2S removal agent. The solvent could be used and regenerated offshore, supported by new technological developments, such as "subsea on a stick" [9].

This work is a first step in the investigation of this multifunctional solvent, with focus on the effect of total pressure in the H_2S removal capacity of the solvent. The measurements were conducted at high pressures, up to 10000 kPa, with methane as the pressurization medium, since it is the main constituent of natural gas. Few researchers have previously studied the effect of high-pressure methane for the systems CH_4—CO_2-MDEA-H_2O [10,11] and CH_4—H_2S-MDEA-H_2O; a detailed literature review for the latter is provided in Section 2.1. The main finding has been that for both CO_2 and H_2S-contained systems, an increase in total pressure leads to increase in the acid gas partial pressure. To our best knowledge, there are no data reported for the system CH_4—H_2S-MDEA-H_2O and MDEA solutions with concentrations higher than 50 wt% MDEA-H_2O.

A 50.1 wt% MDEA-H_2O and a 70 wt% MDEA-H_2O system were used in this work to obtain vapor-liquid equilibrium data (VLE) with hydrogen sulfide and methane. The new VLE data for the system CH_4—H_2S-MDEA-H_2O with 70 wt% MDEA-H_2O mixtures were obtained at temperatures of approximately 283, 353 and 393 K and pressures of 2000, 6000 and 10000 kPa. The experiments were performed isothermally and the temperature of 283 K was chosen to simulate the low-temperature subsea conditions while the temperature of 393 K was chosen to simulate the high regeneration temperature.

2. Literature review

2.1. H_2S-MDEA—H_2O—makeup gas system

An updated list of available VLE data for the system H_2S-MDEA-H_2O, including data with makeup gas, is provided in Table 1. The amine concentration is expressed in a weight basis for all reference sources to allow for direct comparisons. Concentrations reported in molarities [12—14] have been converted to weight fractions using the density correlations presented by Bernal-García et al. [15]. The solution preparation temperature was assumed to be 298.15 K due to lack of this information.

As also other authors working with the system H_2S-MDEA-H_2O have observed, the available data in the literature are rather scattered, especially at low loadings. The literature data have been evaluated for self-consistency and mutual-consistency with reported data in similar experimental conditions, following Chunxi and Fürst's approach [16]. This evaluation was performed in order to decide if some data sets would be excluded during our thermodynamic modeling. During the evaluation, the partial pressures for H_2S from Kuranov et al. [17], Kamps et al. [18] and Sidi-Boumedine et al. [19], who all report total pressures in the absence of makeup gases, were calculated by subtracting the vapor pressure of the solvent calculated by Dalton's Law (Eq. (1)). The vapor pressure of H_2O was calculated by the correlations proposed by NIST for the given temperature ranges while the vapor pressure of MDEA was calculated based on the Antoine correlation fitted to

Table 1
Literature VLE data for H_2S-MDEA-H_2O including data with makeup gas.

wt.% aq. MDEA	T (K)	P_{H2S} (kPa)	P_{tot} (kPa)	Loading	Makeup gas	Analysis Method		Source	NP
						Vapor Phase	Liquid Phase		
11.8, 23.4, 48.9	298.15, 313.15, 323.15, 373.15, 393.15	0.0013 −5890	–	0.00129 −3.229	Nitrogen (P_{H2S} < 200 kPa)	GC	Iodometric back-titration with thiosulfate	Jou et al. [12]	153
11.9, 20	298.15, 310.95, 338.75, 388.75	13.23 −1536.6	–	0.18 −2.1703	–	Mass balance	Mass balance	Bhairi, Maddox et al. [26,27] [c b]	49
23.4	313.15	0.52 −1600	–	0.13 −1.725	–	GC	Iodometric back-titration with thiosulfate	MacGregor and Mather [14] [c b]	27
35, 50	313.15, 373.15	0.00183 −313	–	0.00410 −1.077	Nitrogen (P_{H2S} < 350 kPa)	GC	Iodometric back-titration with thiosulfate	Jou et al. [21] [c]	50
29.9	313.15, 333.15, 353.15, 373.15	1.498 −445.7	–	0.082 −0.902	Nitrogen (P_{H2S} < 200 kPa)	Mass balance (P_{H2S} < 200 kPa)/ GC (P_{H2S} > 200 kPa)	Iodometric back-titration with thiosulfate	Li and Shen [13] [c]	43
23.1, 50	313.15, 343.15, 373.15, 393.15	0.0033 −3673	–	0.00240 −1.74	Nitrogen (P_{H2S} < P_{amb})	Mass balance	Iodometric back-titration with thiosulfate	Huang and Ng [23] [c]	42
23, 50	313.15, 323.15	0.00069 −5.268	96−110	0.00219 −0.313	Nitrogen (P_{H2S} < P_{amb})	FTIR	FTIR	Rogers et al. [24] [c,b]	30
11.83, 23.63	~298.15, ~313.1	0.023 −1.611	–	0.0101 −0.2610	–	Mass balance	Mass balance	Lemoine et al. [28] [c b]	29
18.7, 32.2	313.16, 333.15, 373.15, 393.15, 413.15	–	165.2 −4895.9	0.48 −1.934	–	Mass balance	Mass balance	Kuranov et al. [17] [c b]	71
48.8	313.11, 353.16, 393.15	–	147.9 −2783	0.153 −1.428	–	Mass balance	Mass balance	Kamps et al. [18] [c b]	26
46.78	~313, ~373	–	6.21 −1040	0.039 −1.116	–	Mass balance	Mass balance	Sidi-Boumedine et al. [19] [c,b]	27
23.7	313.2	14−1361	–	0.505 −1.639	–	Mass balance	Mass balance	Zoghi and Shokouhi [22] [c,b]	12
35. 50	283, 298, (313)	0.141 −18.892	690 −6900	0.028 −0.575	Methane	GC	Iodometric back-titration with thiosulfate	Huttenhuis et al. [25]	30
50	323.15	3−278	493 −700	0.096 −0.889[a]	Methane	GC	Mass balance	Dicko et al. [29] [c]	5
50	322.95, 343.15	31−974	1480 −7090	0.267 −1.042	Methane	GC	Titration with silver nitrate	Sadegh et al. [30] [c,b]	39

[a] Global loading.
[b] Reported uncertainty in pressure.
[c] Reported uncertainty in H_2S loading/mole fraction.

Table 2
Literature VLE, FPD and H^E data for the binary system MDEA-H_2O.

Property	wt.% aq. MDEA	$T/\Delta T_F$ (K)	P (kPa)	Source	NP
VLE	3–78.61	313.15–373.15	6.47–100.40	Kim et al. [33]	61
	10–70	326.15–381.15	13.08–101.67	Xu et al. [34]	34
	30–98.9	350.15–458.65	40–66.7	Voutsas et al. [35]	27
FPD	17.4–39.1	(-3.3)-(-13.8)	101.13	Chang et al. [31]	21
	2.6–39.6	(-0.4)-(-14.2)	101.3	Fosbøl et al. [32]	12
H^E	9.6–92.5	298.15–342.45	–	Posey [36]	16
	17.5–96.7	298.15–313.15	–	Maham et al. [37]	26
	41.8–98.4	338.15	–	Maham et al. [38]	9

Table 3
Literature vapor pressure data for pure MDEA.

T (K)	P^s (kPa)	Source	NP
293.69–401.97	0.0006–1.4776	Noll et al. [39]	26
406.69–435.50	2.48–7.98	Kim et al. [33]	7
420.45–513.85	3.68–90.44	Daubert et al. [40]	14
467.39, 479.39, 488.15	20, 30, 40	Yang et al. [41]	3
519.7–738.4	98.59–3985	VonNiederhausern et al. [42]	9

existing and new data as presented in Section 5. **Results and Discussion**.

$$P^s_{solv} = P^s_{MDEA} \cdot x_{MDEA} + P^s_{H_2O} \cdot x_{H_2O} \quad (1)$$

Li and Shen [13] measured H_2S solubility in 29.9 wt% aqueous MDEA at temperatures up to 373 K. During the evaluation of the data, a sharp increase of partial pressure at loadings >0.7 mol H_2S/mol MDEA was noticed, resulting in a cross-over of literature data reported for 35 wt% and 50 wt% MDEA-H_2O solutions. For this reason, the data from Li and Shen [13] were not included in our database used in the model parametrization, as chosen also by Huttenhuis et al. [20].

Jou and coworkers [12,21] have published experimental data for a 48.9 wt% and for a 35 wt% MDEA solution. Two observations can be made for the low loading region: a) the data with a 35 wt% [21] and a 48.9 wt% [12] MDEA solution are very similar and b) the deviations between the data with a 48.9 wt% and a 50 wt% solution look larger than what one would expect with such similar concentrations. Uncertainty information is not available in the first publication of Jou et al. [12], while the authors on their second publication report 3% error in liquid loading and 0.1% full scale (FS) error in pressure. Taking this into account, the deviations related to a) and b) are within the experimental uncertainty. Generally, the data from Jou et al. agree with literature values in different concentrations and temperatures besides at low loadings. For example, good agreement is observed between the data Jou et al. [12] for a 23.4 wt% aqueous MDEA at 313 K and from two other sources [14,22] at loadings > 0.4 mol H_2S/mol MDEA. Any small deviations are justified in terms of reported experimental uncertainties provided by MacGregor and Mather [14] (pressure, loading, composition) as well as by Zoghi and Shokouhi [22] (pressure and composition). At lower loadings, significant deviations are seen between the data by Jou et al. [12] and MacGregor and Mather [14] compared to Huang and Ng [23] as well as Rogers et al. [24]. These differences are difficult to explain by the reported uncertainties only. At higher loadings, some inconsistencies are also seen, for example, the data from Kuranov and coworkers [17] for a 32.3 wt% amine solution are close to the data reported for a 50 wt% MDEA solution [12,23].

No pattern was identified between the analysis method and the uncertainty of the results. Unfortunately, often the uncertainty in loading, which could enlighten the reasons for the scatter observed at low loadings, is not reported. The literature sources reporting uncertainties in either pressure or loading are marked in Table 1. In addition, the differences observed in the reported data could also be attributed to the purity of the chemicals. Although most of the authors report the use relatively high-purity chemicals (>98–99 wt % MDEA, >99 vol% H_2S), the chemical's aging (contamination, contact with atmospheric humidity, light degradation etc.) could also have contributed to the differences observed.

2.2. MDEA-H_2O system

Vapor-liquid equilibrium (VLE), freezing-point depression (FPD) and molar excess enthalpy H^E data for the binary subsystem MDEA-H_2O are given in Table 2. The data were used to model the binary system first in order to reduce the number of parameters to be fitted for the ternary system H_2S-MDEA-H_2O onwards, as it will be further explained later in Section 4. **Thermodynamic modeling**. Eight points from Chang et al. [31] were excluded due to their deviations from the data by Fosbøl et al. [32].

2.3. Pure MDEA

A literature review was also performed for the vapor pressure of MDEA. As seen in Table 3, the data already reported in the literature cover a large range of temperatures, from 293 to 738 K.

3. Experimental work

3.1. Materials

Information for the chemicals used are provided in Table 4. MDEA was used as received from the supplier without further purification. Ultra-pure Millipore water was used in this work to prepare the aqueous amine solutions. Both the amine and the water

Table 4
Chemical sample table.

Component	IUPAC name	CAS	Supplier	Purity	Analysis method
N-methyldiethanolamine (MDEA)	2-[2-hydroxyethyl(methyl) amino] ethanol)	105-59-9	Sigma-Aldrich	≥99 wt%	GC
Water	Oxidane	–	–	Ultra-pure	–
Hydrogen sulfide	Sulfane	7783-06-4	Air Liquide	≥99.5 vol%	GC
Methane	Methane	74-82-8	Air Liquide	≥99.995 vol%	GC

were degassed independently and they were mixed under vacuum to eliminate presence of air during the experiment. The solutions were prepared gravimetrically in a METTLER PM1200 scale with an accuracy of $1 \cdot 10^{-5}$ kg. The composition uncertainty is the same for each component in a binary mixture as explained in Appendix, and it was found to be $u(w) = 0.002$ for 50.1 wt% MDEA-H_2O and $u(w) = 0.003$ for 70 wt% MDEA-H_2O. The gases used in this work are hydrogen sulfide and methane as a makeup gas.

3.2. Experimental set-ups

High-pressure VLE. The high-pressure vapor-liquid equilibrium (VLE) experiments were conducted in an in-house manufacture by ARMINES employing the static-analytic method [43] The apparatus is designed for measurements with acid gases and can be operated in the pressure range from 0.5 to 19.9 MPa and temperatures, from 223 to 473 K. Temperature regulation with an accuracy of ±0.01 K is achieved through immersing the cell into an oil bath. The apparatus is similar to the one previously presented by Ref. [29] and its schematic is given in Fig. 1.

The setup consists of three distinct parts: a) the equipment for filling up the equilibrium cell, i.e. the variable volume press (VVP), the gas bottles and gas tanks, b) the equilibrium cell, including automatic samplers for the gas and the liquid phase(s) and c) the equipment for the analysis of the samples, i.e. the gas chromatograph. Each of these parts consists of various valves and instrumentation. A variable volume press composed by the variable volume pressure cell, a piston and a displacement transducer, was used to introduce the liquid inside the cell, under vacuum. The transducer measures the piston displacement with an accuracy of $\pm 1 \cdot 10^{-5}$ m and, by knowing the dimensions of the cell, the exact volume of the solvent introduced was determined. Approximately $6 \cdot 10^{-6}$ m^3 of solvent were introduced in every experiment. An H_2S bottle was connected to a gas tank with volume of $1.61 \cdot 10^{-4} \pm 5 \cdot 10^{-8}$ m^3, which was further connected to the cell. The presence of a small gas tank between the gas bottle and the cell was dictated as an extra safety barrier in case of leakage of the toxic H_2S. Pressurization of the cell with methane was done directly from the CH_4 bottle.

The equilibrium cell is a sapphire tube standing between two Hastelloy flanges. Kalrez O-rings are used for sealing the tube. The upper flange accommodates two non-rotating stem loading valves, for H_2S and for CH_4, and the lower flange accommodates two more, only one of which was used for the loading of the liquid solution and the discharge of the cell. The temperature is monitored and controlled by two platinum probes and two 100 Ω Platinum resistance temperature detectors (Pt100) with an uncertainty of ±0.02 K. Each of the two located in each flange. They are connected to an HP data acquisition unit and are carefully periodically calibrated. The cell is equipped with two Druck™ pressure transducers, one calibrated for 0–3 MPa and the other for 0–30 MPa pressure range respectively. The transducers are maintained at the temperature they were calibrated at and the uncertainty is 0.6 kPa. The volume of the cell is $33.12 \cdot 10^{-6} \pm 5 \cdot 10^{-8}$ m^3 (or $32.24 \cdot 10^{-6}$ m^3 when the low-pressure transducer is isolated). A stirring system is integrated to the cell in order to reduce the time of equilibration

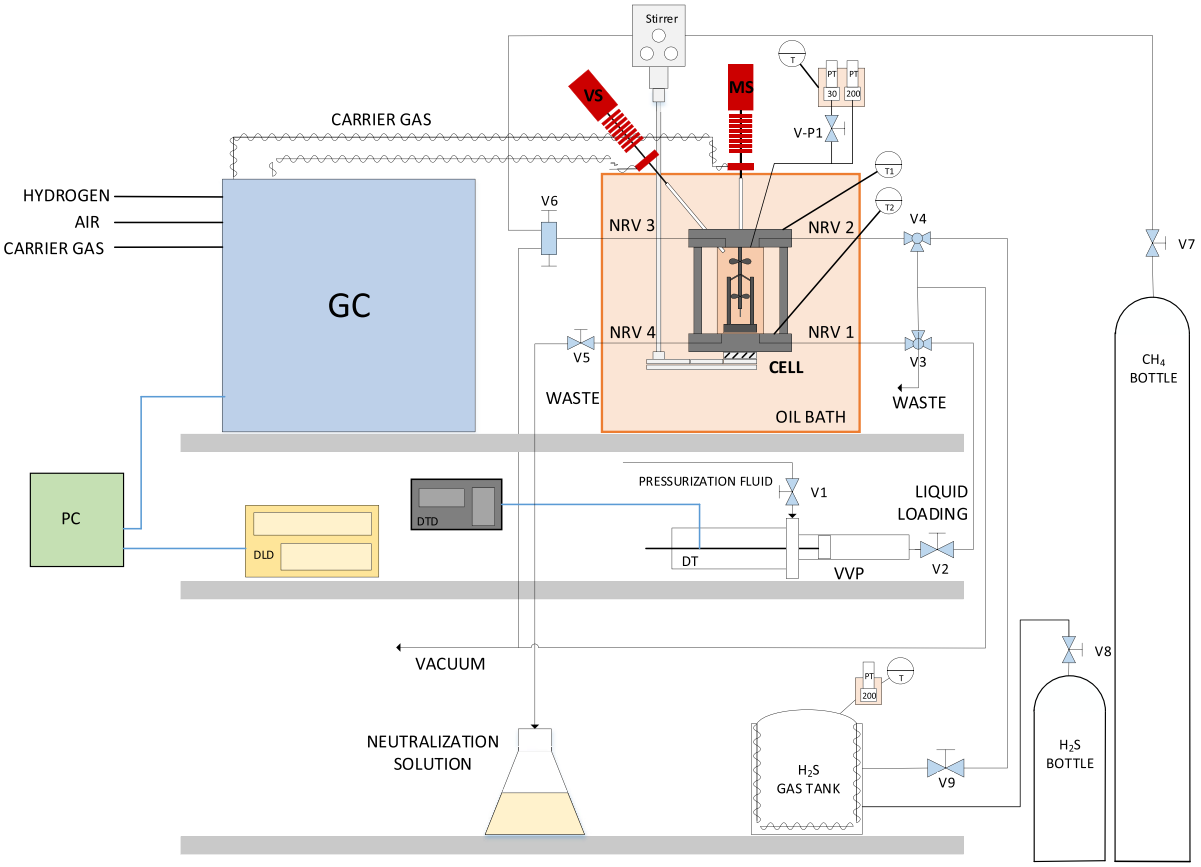

Fig. 1. High-pressure VLE setup. DTD: Displacement Transducer Display, DLD: Data Logging Device, DT: Displacement Transducer, GC: Gas Chromatograph, MS: Mobile Sampler for the analysis of liquid phase, NRV: Non-Rotating valve, PC: Personal Computer for data acquisition, PT: Pressure Transducer, T: Thermocouple, V: Valve, VS: Vapor Sampler for the analysis of gas phase, VVP: variable volume press.

and ensure phase homogeneity. The variable-speed stirrer is composed by a rotating axis inside the cell, two propellers mounted on the rotating axis for stirring both the gas phase and the liquid phase and a magnetic rod mounted on the rotating axis in order to allow for rotation of the axis by a stirring motor located below the cell.

Agilent software BenchLink is used for online monitoring of pressure and temperature, enabling the determination of equilibrium. Once the equilibrium is reached, micro samples can be withdrawn and transferred to the GC for analysis. Automatic sampling is allowed through two capillary samplers (ROLSI®) Armines' patent [44]. Two capillaries are fixed in the cylindrical wall of the cell at levels designed to withdraw vapor and liquid phase samples. The samplers are connected to a PERICHROM model PR-2100 gas chromatograph, through a heated transfer line. The temperature selected is higher than the boiling point of the heaviest component (MDEA) to avoid any sample condensation. The chromatograph is equipped with a thermal conductivity detector (TCD) and a flame ionization detector (FID), and WINILAB III software is used for GC acquisition and treatment.

Ebulliometer. A modified Swietoslawski ebulliometer was used, described earlier in detail by Kim et al. [33]. The apparatus can be operated at temperatures up to 473 K and at sub-atmospheric and atmospheric pressure. The temperatures were measured with calibrated Pt100 resistance thermosensors with an uncertainty of ±0.05 K. A DP1520 pressure controller from Druck™ was used, calibrated against a BeamexC5 calibrator with an accuracy of ±0.03 kPa. The solution is accommodated inside a $2 \cdot 10^{-4}$ m^3 glass equilibrium still and the set-up allows for the sampling of both the vapor and the liquid phase.

3.3. Experimental procedure

High-pressure VLE. After thorough cleaning with hot deionized (DI) water and ethanol, the cell and tubings were left to dry and set to vacuum during the previous night. The solution was prepared under vacuum directly inside the VVP and the solution preparation temperature was approximately 298 K. Back-pressure of ca. 500 kPa of methane was applied to the VVP. The solution was introduced inside the cell, and the end displacement position was recorded, so as the exact amount of solution added could be calculated. The cell was immersed into the bath, the stirrer was turned on, the temperature of the experiment was set and the system was left to equilibrate. Temperature stabilization required approximately 30–60 min, after which the vapor pressure of the solution was recorded.

The desired global loading, i.e. mol of H_2S inside the cell per mol of amine, was first decided and based on the PVT conditions of the H_2S gas tank before and after the filling of the cell, the amount of H_2S introduced was determined. The calculations were performed using REFPROP software [45] and a Helmholtz energy-based equation of state developed by Ref. [46] for pure H_2S was used. The global loading was, thus, calculated by:

$$n_{H2S} = n^{before}_{H2S,tank} - n^{after}_{H2S,tank} \tag{2}$$

$$\alpha_{glob} = \frac{n_{H2S}}{n_{MDEA}} \tag{3}$$

For the experiments with the 50.1 wt% MDEA aqueous solution, initially a small amount of H_2S was introduced and it was left to equilibrate. Reaction of H_2S and MDEA is fast and equilibrium was reached within 1 h. Because the total pressure was lower than the minimum required pressure of 500 kPa for the ROLSI® samplers and GC to function, methane was added up to 500 kPa. Equilibrium was reached in approximately 1 h, and the sampling started. In our experiments, sampling and analysis was conducted only for the vapor phase. Higher loadings were reached by adding more H_2S into the cell and repeating the above-mentioned procedure.

For the 70 wt% MDEA solution VLE investigation, two series of experiments were conducted based on the global loading, one for 0.2 and one for 0.5 mol H_2S/mol MDEA approximately. The experimental procedure varies in the way that after equilibrium was reached, methane was added in 3 stages, up to 2000, 6000 and 10000 kPa. At each pressure level, sampling and analysis of the vapor phase was performed upon equilibrium. The experiments were performed under isothermal conditions, at 283, 353 and 393 K. At the end of the experiment, the cell was depressurized and emptied safely through a caustic solution (NaOH) in order to neutralize the system. At each temperature, a new experiment was conducted using fresh solution. We aimed at having the same global loading at all temperatures, however it was not practically possible to reach exactly the same loadings in every experiment. The study at each temperature and global loading lasted approximately one week.

The analysis of vapor phase concentration was performed in a GC equipped with a Porapak-R column R80/100 mesh (length 2 m, diameter 2 mm) from RESTEK. The carrier gas was helium at a flow rate of 20 ml/min. A constant temperature program at 363 K was used for the quantification of both methane and hydrogen sulfide. Analysis at 383 K was also performed to check for water presence in the vapor phase. In order to check the repeatability of the measurements and to perform uncertainty analysis, five samples at least were withdrawn, the first two of them usually were required to saturate the transfer lines in terms of adsorption. Disturbance to equilibrium was considered negligible due to the small volume of each sample.

Knowing the pressure, temperature and the composition of the vapor phase, the density of the vapor phase was estimated using REFPROP software [45]. The amount of n_{H2S} in the vapor and liquid phase and finally the H_2S loading in the liquid phase, liquid loading α, were calculated according to Eq. (4) - Eq. (7).

$$n^v_{tot} = \rho^v \cdot V^v \tag{4}$$

$$n^v_i = n^v_{tot} \cdot y_i \tag{5}$$

$$n^l_i = n_{tot} - n^v_i \tag{6}$$

$$\alpha = \frac{n^l_{H2S}}{n_{MDEA}} \tag{7}$$

where ρ^v is the molar density of the gas mixture, calculated using REFPPROP and V^v is the volume of the vapor phase. The latter is the difference between the volume of the cell, ca. $33 \cdot 10^{-6}$ m^3, which is known from our calibration data and the volume of the liquid which was estimated by the correlations proposed by Ref. [15], assuming that the effect of pressure in the liquid volume is negligible. Bernal-García and coworkers measured the density of aqueous MDEA in the whole composition range at temperature range of 263.15–363.15 K and, based on their data, calculated the excess molar volumes of the binary systems. For our calculations at the temperature of 393 K which was not studied in the aforementioned work, the excess molar volume was extrapolated. It is worth mentioning that the deviations in number of moles of H_2S calculated by the Ideal Gas Law equation and REFPROP employing the most up-to-date Helmholtz energy-based EoS led to deviations in the liquid loading lower than 1.5% at 283 and 353 K, while the deviations were higher at 393 K (max 2.7%). For more accurate

results, we used the results based on the latter.

Ebulliometer. Approximately $0.8 \cdot 10^{-4}$ m^3 of liquid was charged inside the still, preceding purge with nitrogen. The desired temperature was set and equilibrium was assumed after 10 min of stable pressure and temperature. The vapor pressure of MDEA was measured at the temperature range of 405–435 K. Validation of the apparatus was performed by measuring the vapor pressure of water and a 1.5% maximum error from the literature was found in equilibrium pressure.

4. Thermodynamic modeling

High pressure VLE. An in-house MATLAB-based rigorous model has been developed to describe the chemical and phase equilibrium for the system H_2S-MDEA-H_2O. The same algorithm has been previously used to successfully describe CO_2-amine-H_2O systems relevant to carbon capture processes [47,48]. Peng-Robinson EoS [49] with the original alpha function was employed to describe the non-idealities of the vapor phase, coupled with the traditional van der Waals one-fluid mixing rules. The binary interaction parameters for Peng-Robinson EoS in this work were set to zero. To account for the non-idealities in the liquid phase, the electrolyte non-random two-liquid (eNRTL) model [50] was utilized. The models are presented in the Appendix. The required critical parameters and acentric factors for pure components are given in Supplementary Information (Section A).

The chemical reactions assumed in the liquid phase are the ionization of water, the protonation of MDEA and the dissociation of H_2S (R. 1-3). The second dissociation reaction of hydrogen sulfide, from bisulfide to sulfide, is not considered in our model due to the low concentration of S^{2-} in the solution and in order to reduce the number of parameters in the model [16].

$$2\ H_2O = OH^- + H_3O^+ \quad \text{(R.1)}$$

$$MDEA + H_3O^+ = MDEAH^+ + H_2O \quad \text{(R.2)}$$

$$H_2S + H_2O = H_3O^+ + HS^- \quad \text{(R.3)}$$

The chemical equilibrium constants as well as Henry's constant for hydrogen sulfide are described by Eq. (8), parametrized according to Table 5, where x stands for either the chemical equilibrium constant K_{eq} or Henry's constant H_{H2S}. Temperature is expressed in K and Henry's constant for hydrogen sulfide in kg·atm.

$$\ln(x) = A + \frac{B}{T} + C\ln(T) + DT \quad (8)$$

The vapor pressure for hydrogen sulfide and water is estimated using the Riedel correlation (Eq. (9)) where T expressed in K and P^{sat} in Pa. The parameters are presented in Table 6. MDEA vapor pressure has been measured in this work and fitted to Antoine correlation. The Antoine parameters used in this work can be found in Section 1.5.2.

Table 6
Parameters for pure component vapor pressure correlations for Eq. (9).

Component	Model	A	B	C	D	E	Reference
H_2S	Riedel	106.47	−5018	−13.306	−0.09	−0.13	DIPPR [53]
H_2O	Riedel	73.649	−7258	−7.304	4.2E-06	2	DIPPR [53]

$$\ln(P^{sat}) = A + \frac{B}{T} + C\ln(T) + DT^E \quad (9)$$

A sensitivity analysis was performed to evaluate the significant numbers in the parameters retrieved from the literature. In Tables 5 and 6 the parameters are provided only with their significant digits.

The adjustable parameters for the eNRTL model are the non-randomness factors, α, and the energy parameters, τ_{ij}. The optimization of the H_2S-MDEA-H_2O system requires the regression of a total of 78 parameters. In order to reduce this high number of parameters to be adjusted, the following steps have been taken:

I) All non-randomness factors α have been given fixed values according to Table 7.
II) The energy parameters for the subsystem H_2S–H_2O have been fixed to the default values used in Aspen Plus V10 simulation software (Table 7).
III) The energy parameters for the subsystem MDEA-H_2O have been fixed to the values obtained by the regression of the literature data presented in Subsection 2.2 **MDEA-H_2O system.**

As a result, the number of parameters is reduced to 36. The temperature dependency of the energy parameters is described by Eq. (10), where a_{ij} and b_{ij} were fitted to experimental data.

$$\tau_{ij} = a_{ij} + \frac{b_{ij}}{T} \quad (10)$$

The fixed non-randomness factors and fixed energy parameter values are presented in Table 7, where m denotes molecule and c-a cation-anion (salt). The non-randomness factors were fixed at 0.2 for molecule-molecule and water-salt interactions, and at 0.1 for the H_2S-salt and MDEA-salt interactions, according to Hessen and coworkers [54].

The optimization routine used in this work is Particle Swarm Optimization (PSO), developed by Kennedy and Eberhart [55]. This algorithm allows for the optimization of continuous non-linear functions, using particle swarm methodology. The advantage of this optimization routine is that it uses random initialization, thus, unlike other optimization methods, its convergence is not dependent on the first approximations. In order to avoid local minima and find an optimal solution, local best topology was used [56,57]. The PSO parameters are swarm size of 40, maximum number of iterations 600 in 3 loops which terminate once the optimized value deviates more than 10^{-4} (tolerance criterion) from its preceding one or if less than 1% improvement is achieved during 60 iterations. The minimization of the absolute average relative deviation (AARD)

Table 5
Mole fraction-based parameters for Eq. (8), reported only with their significant digits.

	A	B	C	D	Reference
Chemical Equilibrium constant for R. 1	132.89	−13445	−22.477	0	Posey [36]
Chemical Equilibrium constant for R. 2	−60.03	−1974	7.533	0	Oscarson et al. [51]
Chemical Equilibrium constant for R. 3	214.58	−12995	−33.547	0	Posey [36]
Henry's constant for H_2S	342.595	−13237	−55.0551	0.05957	Edwards et al. [52]

Table 7
Fixed parameters of eNRTL model used in this work.

Non-randomness factors, α					
Components					
i	j	ij	ji	–	–
m	m	0.2	0.2		
H_2O	c-a	0.2	0.2		
H_2S	c-a	0.1	0.1		
MDEA	c-a	0.1	0.1		

Energy parameters, τ_{ij}					
Components		a		b	
i	j	ij	ji	ij	ji
H_2O	H_2S	0	0	0	0
H_2O	H_3O^+-OH^-	8	−4	0	0
H_2O	H_3O^+-HS^-	8	−4	0	0
H_2S	H_3O^+-OH^-	15	−8	0	0
H_2S	H_3O^+-HS^-	15	−8	0	0

shown in Eq. (11), was chosen as the objective function, where Y was either the partial pressure of H_2S, $P_{H2S,}$ or the total pressure, P_{tot}.

$$F_{obj}(\%) = \frac{1}{N}\sum_{i}^{N}\frac{\left|Y_i^{exp} - Y_i^{pred}\right|}{Y_i^{exp}}\cdot 100 \quad (11)$$

5. Results and Discussion

5.1. Experimental results

High-pressure VLE. The experimental vapor-liquid equilibrium data obtained in this work with 50.1 wt% and 70 wt% MDEA solution for the system CH_4−H_2S-MDEA-H_2O at various pressures and temperatures are presented in Table 8 and Table 9. As mentioned earlier, knowing the experimental uncertainty of reported data could possibly help us understand the scatter observed in the data for the system H_2S-MDEA-H_2O. Therefore, we performed a thorough investigation of our measurements' uncertainty in order to properly evaluate our data and conclude on the impact of experimental uncertainty on our results.

We have reported the combined uncertainties employing the Law of propagation of uncertainty according to NIST guidelines [58]. The new data are accompanied by the standard uncertainties for total pressure and temperature as well as the combined uncertainties for the partial pressure of hydrogen sulfide, the global and the liquid loading. It was found that the main contributor to the uncertainty of the partial pressure of H_2S is the total pressure of the system, as can be observed by the increasing uncertainty of P_{H2S} for increasing total pressure. The main contribution to the global loading uncertainty is associated with the loading itself, while the uncertainty of the liquid loading is mostly affected by the uncertainty of the total moles of H_2S introduced in the cell. The repeatability of our measurements was taken into account by virtue of the multiple samples analyzed on the GC at each equilibrium pressure and temperature. The complete uncertainty analysis can be found in Supplementary Information.

Table 8 and Fig. 2 reveal information regarding both the reproducibility of the measurements in this work as well as their comparison with the literature for the system CH_4−H_2S-MDEA-H_2O with a 50−50.1 wt% MDEA solution at approximately 323 K. The measured vapor fractions of methane and hydrogen sulfide are reported in Supplementary Information together with the uncertainty analysis. Our measurements in the presence of 500 kPa of methane were performed in two different experiments, and as one can observe in the figure, the same behavior is followed and the measurements can be reproduced. The data obtained in this work are in agreement with the data reported by Dicko et al. [29] under

Table 8
Experimental vapor-liquid equilibrium data and their corresponding combined uncertainties at total pressure of 500 kPa (and one measurement at total pressure 3000 kPa) and temperature of 323 K for the system CH_4−H_2S-MDEA-H_2O and 50.1 wt% aqueous MDEA[a]. Methane is used as makeup gas.

T	P_{tot}	P_{H2S}	$u_c(P_{H2S})$	α_{glob}	$u_c(\alpha_{glob})$	α_{liq}	$u_c(\alpha_{liq})$	NS
K	kPa	kPa	kPa	mol H_2S global/mol MDEA	mol H_2S global/mol MDEA	mol H_2S liquid/mol MDEA	mol H_2S liquid/mol MDEA	
					Experiment 1			
322.98	493.81	2.99	0.03	0.096	0.003	0.095	0.001	9
322.98	480.01	11.27	0.12	0.214	0.005	0.211	0.002	9
322.98	500.72	49.11	0.43	0.490	0.005	0.477	0.002	7
322.98	604.01	177.59	1.20	0.822	0.006	0.775	0.003	10
					Experiment 2			
322.98	493.92	2.60	0.02	0.085	0.003	0.084	0.002	6
322.98	493.50	22.33	0.19	0.312	0.004	0.303	0.002	6
322.98	498.13	72.79	0.56	0.588	0.006	0.559	0.003	8
322.98	530.82	139.10	0.93	0.760	0.013	0.703	0.006	5
322.98	545.53	168.46	1.06	0.820	0.039	0.751	0.020	9
322.98	3106.96	179.67	1.52	0.820	0.039	0.745	0.020	8

[a] Standard uncertainties not included above are $u(T) = 0.02$ K, $u(P) = 0.6$ kPa.

Table 9
Experimental vapor-liquid equilibrium data and their corresponding combined uncertainties as a function of total pressure and temperature for the system CH_4–H_2S-MDEA-H_2O and 70 wt% aqueous MDEA[a]. Methane is used as makeup gas.

T	P_{tot}	P_{H2S}	$u_c(P_{H2S})$	α_{glob}	$u_c(\alpha_{glob})$	α_{liq}	$u_c(\alpha_{liq})$	NS
K	kPa	kPa	kPa	mol H_2S global/mol MDEA	mol H_2S global/mol MDEA	mol H_2S liquid/mol MDEA	mol H_2S liquid/mol MDEA	
283.00	2011.87	3.48	0.03	0.232	0.003	0.231	0.003	9
283.00	6030.85	3.85	0.05	0.232	0.003	0.231	0.003	10
283.00	10052.50	4.68	0.04	0.232	0.003	0.231	0.003	7
352.99	1976.07	106.23	0.92	0.239	0.002	0.211	0.002	5
352.99	3954.66	108.30	0.98	0.239	0.002	0.210	0.002	10
352.99	5957.76	108.03	1.03	0.239	0.002	0.210	0.002	7
352.99	7976.36	111.95	1.04	0.239	0.002	0.209	0.002	6
352.99	9988.18	111.42	1.12	0.239	0.002	0.208	0.002	6
393.00	2024.40	375.10	1.46	0.246	0.002	0.167	0.002	8
392.99	5979.36	376.17	1.72	0.246	0.002	0.165	0.002	10
393.00	9925.29	364.18	1.97	0.246	0.002	0.167	0.002	8
283.00	1975.74	13.13	0.15	0.488	0.002	0.484	0.002	7
283.00	5990.55	17.37	0.28	0.488	0.002	0.482	0.002	5
283.00	10045.17	21.56	0.24	0.488	0.002	0.480	0.002	6
352.92	2006.00	264.36	1.30	0.478	0.002	0.415	0.002	7
352.92	5980.37	281.97	1.57	0.478	0.002	0.408	0.002	8
352.92	9975.23	300.30	1.67	0.478	0.002	0.402	0.002	8
393.05	974.22	834.43	0.49	0.484	0.002	0.304	0.003	3
393.00	2034.17	818.12	2.26	0.484	0.002	0.308	0.003	8
393.01	5893.45	806.74	3.34	0.484	0.002	0.309	0.003	7
393.00	9915.85	809.32	3.68	0.484	0.002	0.307	0.003	9

[a] Standard uncertainties not included above are $u(T) = 0.02$ K, $u(P) = 0.6$ kPa.

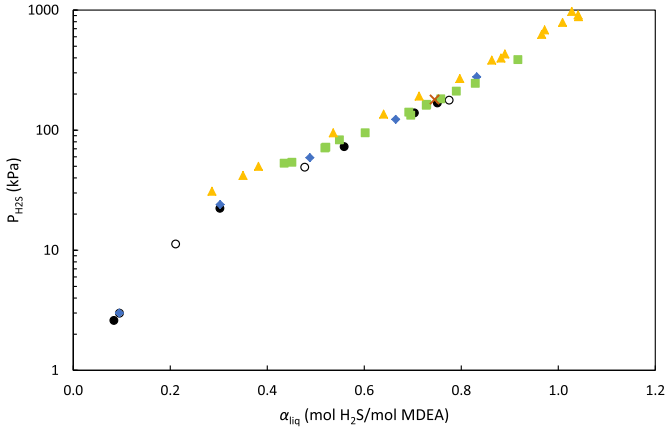

Fig. 2. Equilibrium H_2S partial pressures as a function of liquid loading and total pressure for 50 wt% MDEA-H_2O at 323 K. ● P_{tot} = 500 kPa (This work, Experiment 1), ○ P_{tot} = 500–600 kPa (This work, Experiment 2), ♦ P_{tot} = 500–700 kPa [29], ■ P_{tot} = 1500 kPa [30], × P_{tot} = 3000 kPa (This work), ▲ P_{tot} = 7000 kPa [30].

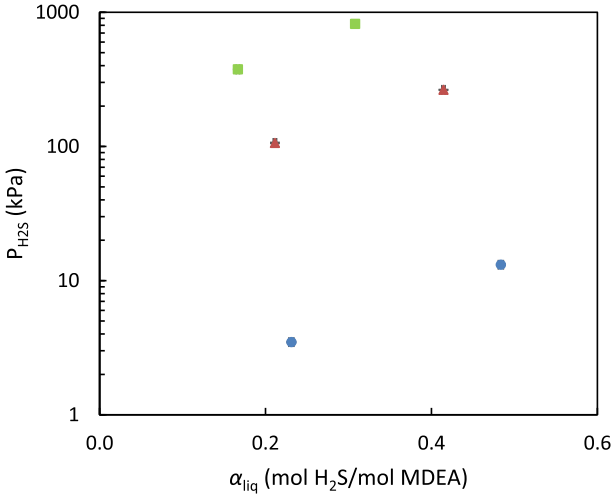

Fig. 3. Experimental H_2S solubility in a 70 wt% MDEA-H_2O system with methane as makeup gas at total pressure of 2000 kPa at temperature; ● 283 K, ▲ 353 K and ■ 393 K. Error bars for both H_2S partial pressure and loading are included.

similar conditions. These data together with Sadegh et al.'s data [30] at total pressure of 1500 kPa and 7000 kPa show that, for a given liquid loading, an increase in the total pressure of the system leads to an increase in the H_2S partial pressure. Our single measurement at total pressure of 3000 kPa for this system follows this trend, too. An exception is the last point reported by Dicko et al. at α_{liq} = 0.832 mol H_2S/mol MDEA, which also differs from the trend in our data. This point is measured at total pressure 700 kPa but lies between the data reported by Sadegh et al., at 1500 kPa and 7000 kPa total pressure. Here it is important to mention that the measurements reported by Dicko et al. are global loadings, and the liquid loadings shown in Fig. 2 are the ones calculated by the authors.

The observation of increased H_2S partial pressure upon increase in total pressure can be made also for the 70 wt% aqueous MDEA system for the temperatures of 283 K and 353 K. The deviations in partial pressure are higher for higher global loadings. On the other hand, the liquid loading remains unchanged at 283 K while the one at 353 K seems to decrease. At 393 K, not clear trends are shown. This behavior is noticed for all global loadings, though the fact that the water present in the vapor phase could not be quantified through the GC analysis, and it was therefore calculated based on the vapor pressure of the solvent under the assumption that it was constant with increasing total pressures, might have its share on

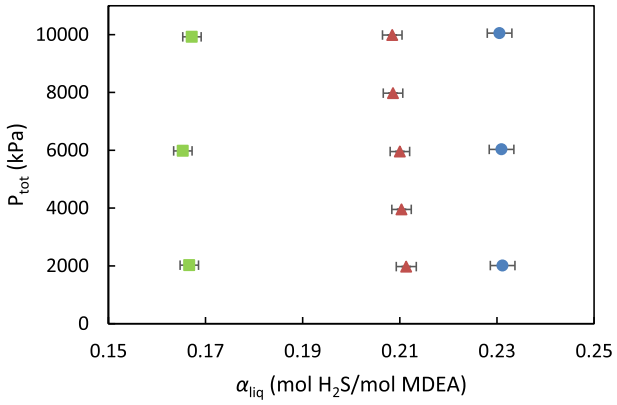

Fig. 4. H_2S liquid phase loading of a 70 wt% MDEA-H_2O system with methane as makeup gas as a function of total pressure and temperature; ● 283 K, ▲ 353 K and ■ 393 K. Error bars for both total pressure and liquid loading are included.

the latter. The effect of temperature is the expected one given the exothermic nature of the chemical reactions; the lower the temperature, the higher the absorption of H_2S in the liquid phase at constant partial pressure of hydrogen sulfide. The features discussed above are illustrated in Fig. 3 and Fig. 4. It is worth mentioning that error bars representing the uncertainty in pressures and loadings are included in the figures, however uncertainties in pressure are too low to be visible.

Although there is a clear trend of the pressure effect on the partial pressure of H_2S, taking into account the uncertainties, it can be seen that the deviations in liquid loading are similar to the experimental uncertainty. In fact, at 283 K and for global loading 0.232, no change at all in liquid loading is observed. The fact that hydrogen sulfide is chemically bound to the amine reinforces the argument that the differences in loading are due to uncertainty in measurements. The amount of methane dissolved in the liquid phase is too low to have an impact on the reaction of hydrogen sulfide with the amine solution which is an exothermic reaction whose reversion requires high amounts of energy. Overall, it is observed that the effect of increasing the total pressure from 2000 kPa to 10000 kPa in terms of H_2S loading in a 70 wt% aqueous MDEA at temperatures of 283 K, 353 K and 393 K is not significant and, in most cases, it is within or very close to experimental uncertainty.

As Sadegh et al. [30] showed, taking into account the gas

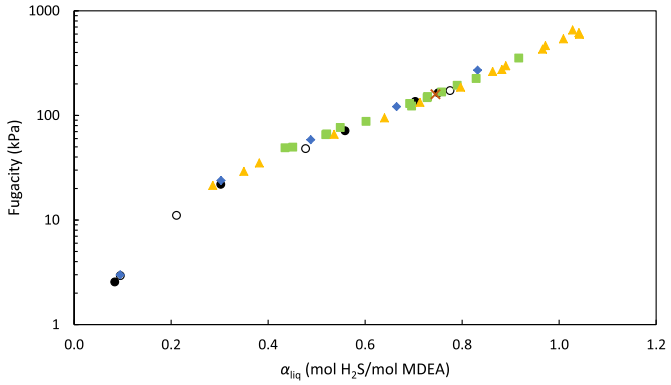

Fig. 5. Equilibrium H_2S fugacities as a function of liquid loading and total pressure for 50 wt% MDEA-H_2O at 323 K. ● P_{tot} = 500 kPa (This work, Experiment 1), ○ P_{tot} = 500–600 kPa (This work, Experiment 2), ♦ P_{tot} = 500–700 kPa [29], ■ P_{tot} = 1500 kPa [30], × P_{tot} = 3000 kPa (This work, Experiment 2), ▲ P_{tot} = 7000 kPa [30].

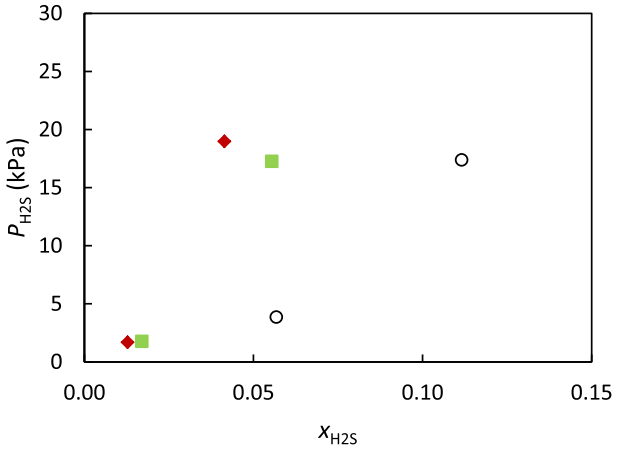

Fig. 6. Hydrogen sulfide molar concentration in the liquid phase for the system CH_4–H_2S-MDEA-H_2O as a function of partial pressure and amine concentration at total pressures 6000–6900 kPa and at 283 K; ♦ 35 wt% MDEA-H_2O [25], ■ 50 wt% MDEA-H_2O [25], ○ 70 wt% MDEA-H_2O (This work).

fugacities is adequate to explain the deviations of the equilibrium H_2S pressures at different total pressures for a 50 wt% aqueous MDEA. Indeed, Fig. 5 shows how the fugacity exhibits the same behavior for all data obtained in a 50–50.1 wt% MDEA-H_2O solution in the presence of methane from different literature sources. The figure is similar to one provided by Sadegh et al. [30], this time enriched with our data at total pressure of 500 and 3000 kPa demonstrating the same behavior. The fugacities were calculated using Peng-Robinson EoS with binary interaction parameters set to zero. As far as the data obtained for the 70 wt% aqueous MDEA are concerned, the fugacity can explain the partial pressure trend observed for our data at 283 K and 353 K. At 393 K, the uncertainty in liquid loadings are such that no solid conclusions can be drawn.

The effect of amine concentration was also studied by means of comparison with reported data in the literature at 283 K and 393 K, shown in Fig. 6 and Fig. 7 respectively. Data at 353 K in our range of loading and pressure are not available in the literature, therefore no comparison could be performed. A clear effect of increasing molar concentration with increasing amine concentration and constant H_2S pressure can be seen in the comparison performed at 283 K. This can be expected since the more amine available, the higher the capacity of the solvent. It is important to state that the literature data are reported only from one reference source [25] where methane makeup gas was also used. Because of the effect of methane presence, we have plotted the available data at similar total pressures; our data only for total pressure of 6000 kPa and the literature data at total pressure of 6900 kPa in order to allow for a fairer comparison. The molar concentration of H_2S is also increasing with amine content in the solution at 393 K, but only up to 50 wt%. Our data at 70 wt% overlap with the literature data obtained in a 50 wt% aqueous MDEA study. This is illustrated in Fig. 7 where we have only plotted the data with very little methane or with total pressure of 2000 kPa from our work.

Hydrogen sulfide can react directly with MDEA through a typical acid-base reaction [2]. At the same time, the presence of water would enhance the acid gas uptake through the dissolution of hydrogen sulfide as well the protonation of the amine. Therefore, we could identify two possible mechanisms through which H_2S is absorbed; one directly into the amine and one via water. Moreover, hydrogen sulfide absorption in MDEA-H_2O is the result of both physical and chemical absorption. Therefore, in order to provide a good discussion about the behavior observed in Figs. 6 and 7, the physical absorption of hydrogen sulfide into MDEA-H_2O systems

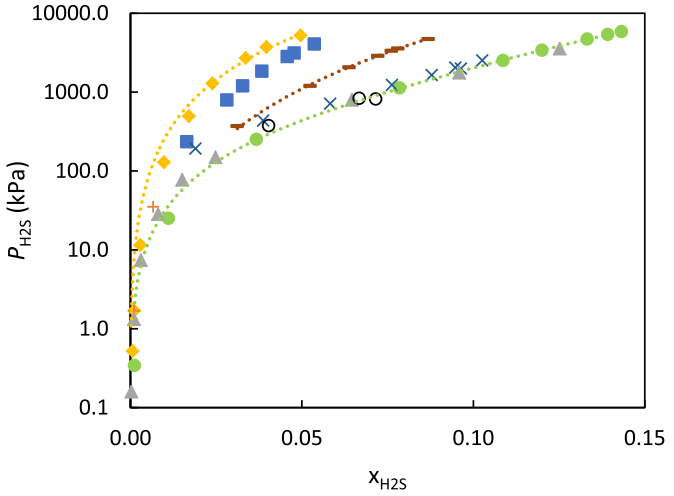

Fig. 7. Hydrogen sulfide molar concentration in the liquid phase for the system H_2S-MDEA-H_2O as a function of partial pressure and amine concentration at 393 K; ♦ 11.8 wt% MDEA-H_2O [12], ■ 18.7 wt% MDEA-H_2O [17], + 23.1 wt% MDEA-H_2O [23], — 32.2 wt% MDEA-H_2O [17], ● 48.8 wt% MDEA-H_2O [12], × 48.8 wt% MDEA-H_2O, ▲ 50 wt % MDEA-H_2O [23], ○ 70 wt% MDEA-H_2O (This work).

should be taken into account. To our best knowledge, only Rinker and Sandall [59] have reported such information. They measured H_2S solubility in protonated aqueous MDEA and their measurements showed that the solubility increases with amine content. Although the available data cover 0–50 wt% MDEA-H_2O systems, it can be assumed that the same trends would be followed and the physical absorption of H_2S in to a 70 wt% aqueous MDEA is higher than in a 50 wt% aqueous MDEA.

Based on the above, the fact that x_{H2S} is not increased with amine content from 50 to 70 wt% at 393 K and constant H_2S pressure indicates that the contribution of the chemical absorption decreases as the amine content increases. This can be also confirmed by observing the slope of indicative tendency curves in Fig. 7 (better illustrated in Fig. S7 in Supplementary Information, where non-logarithmic scale is used for the y axis). The slope reveals information about the absorption capacity of the systems. It is observed that as the amine composition increases, the *P-x* curve has a lower slope (apparent Henry's constant). The lower the slope, the closer to linearity and, thus, higher physical absorption. For example, at 500 kPa, the apparent Henry's constant is 535 kPa m^3/kmol for 11.8 wt% MDEA-H_2O and 300 kPa m^3/kmol for 48.8 wt% MDEA-H_2O at 393 K. This behavior is followed also at higher pressure; at 3000 kPa, the apparent Henry's constant is 1169 kPa m^3/kmol for 11.8 wt% MDEA-H_2O and 715 kPa m^3/kmol for 48.8 wt% MDEA-H_2O at 393 K. Unfortunately, our data are too few to assess the *P-x* linearity for 70 wt% MDEA-H_2O, nonetheless it can be said that the chemical contribution in the overall H_2S uptake is decreased. In the case of low temperatures such as in our studied temperature of 283 K, these effects could probably not be visible because the absorption capacity is very high and our data as well as the data reported in the literature are produced for low H_2S partial pressure.

Table 10
Experimental vapor pressure P^s/kPa for pure MDEA[a].

T (K)	P^s (kPa)				
	Experimental	DIPPR		This work (Table 11)	
		Predicted	ARD (%)[b]	Predicted	ARD (%)[b]
405.34	1.79	1.95	9%	1.79	0%
411.00	2.29	2.53	10%	2.34	2%
415.31	2.79	3.06	10%	2.86	2%
418.58	3.29	3.54	7%	3.31	1%
421.73	3.79	4.05	7%	3.80	0%
424.52	4.29	4.55	6%	4.28	0%
427.21	4.79	5.09	6%	4.80	0%
429.49	5.29	5.59	6%	5.28	0%
431.60	5.79	6.08	5%	5.76	0%
433.49	6.29	6.56	4%	6.22	1%
435.34	6.79	7.05	4%	6.71	1%

[a] Standard uncertainties are u(T) = 0.1 K, u(P) = 0.1 kPa.

[b] ARD (%) = $\frac{\left|P_s^{pred} - P_s^{exp}\right|}{P_s^{exp}} \cdot 100$

Table 11
Parameters for the Antoine correlation for pure MDEA vapor pressure[a].

	A	B	C
MDEA	9.676 ± 0.014	−1965.6 ± 8.9	−99.33 ± 0.69

[a] $\log_{10}P^s = A + \frac{B}{T+C}$. T in K. P in Pa. Temperature range: 294–738 K.

Table 12
AARDs for the fitted P_{tot}, FPD and H^E for the MDEA-H_2O system.

Variable	Source	AARD (%)
P_{tot}	Kim et al. [33]	1.1
	Xu et al. [34]	1.9
	Voutsas et al. [35]	6.4
	Overall	**2.5**
FPD	Chang et al. [31]	10.3
	Fosbøl et al. [32]	4.4
	Overall	**6.0**
H^E	Posey [36]	7.6
	Maham et al. [37]	3.1
	Maham et al. [38]	11.5
	Overall	**7.4**

Ebulliometer. The measurements conducted in the ebulliometer are shown in Table 10. The main limitation of ebulliometric measurements is the absence of stirring. Experimental measurement of the vapor pressure of the binary mixtures used in this work was not possible because two phases formed, associated with the high viscosity of pure MDEA, i.e. ca. 77 mPa s at 298.15 K [60–62]. Therefore, only the vapor pressure of MDEA was measured.

5.2. Modeling results

In this section, we present first the results from the ebulliometer following by the modeling results for the high-pressure VLE data, since the first ones are used in the model parametrization for the H_2S-MDEA-H_2O equilibrium.

Ebulliometer. The Antoine correlation was fitted to available data from the literature (Table 3) as well as the newly obtained data of this work, covering a large range of temperatures and pressures. In Table 10, our experimental measurements are compared with the predicted vapor pressures by our fitted Antoine correlation and the DIPPR equation. At the temperature range of 405–435 K studied in this work, the absolute relative deviation (ARD) between the experimental and the estimated value is 7% with DIPPR equation and 1% in our correlation, which has been fitted to available data in the literature covering temperatures from 293 K to 738 K. The new parameters for Antoine correlation proposed for the estimation of the vapor pressure of MDEA, are shown in Table 11. The Average Absolute Relative Deviation (AARD) is 4% for our correlation and 30% for DIPPR. The high deviation for DIPPR equation is mainly due to the vapor pressure predictions at temperatures higher than 530 K, which explains the high AARD. In the fitting, we excluded

Table 13
BIAS[a], AADs[b] and AARDs[c] for the fitted total pressures, P_{tot}, and H_2S partial pressures, P_{H2S}, for Cases A, B and C.

Source	Case A				Case B				Case C			
	Pressure range	Bias	AAD	AARD	Pressure range	Bias	AAD	AARD	Pressure range	Bias	AAD	AARD
	kPa	(%)	kPa	(%)	kPa	(%)	kPa	(%)	kPa	(%)	kPa	(%)
						Partial pressure, P_{H2S}						
Lemoine et al. [28]	0.023–1.611	−42.8	0.1	42.8	0.176–1.611	−27.0	0.2	27.0	0.176–1.611	−23.7	0.1	23.7
Huang and Ng [23]	0.0033–3673	−32.7	80.4	38.8	2.34–3673	−5.0	82.9	8.6	2.34–3673	−2.5	69.0	13.3
Rogers et al. [24]	0.00069–5.268	−25.7	0.1	32.2	0.2–5.268	−12.1	0.2	13.0	0.2–5.268	−6.8	0.2	12.3
MacGregor and Mather [14]	0.52–1600	48.4	19.3	48.7	0.52–1600	36.6	11.5	37.7	0.52–1600	49.0	15.8	49.2
Jou et al. [21]	0.00183–313	−8.1	5.9	23.6	0.295–313	−2.0	3.6	13.0	0.295–313	6.1	5.9	13.4
Jou et al. [12]	0.0013–5890	18.2	125.6	29.7	0.0273–5890	9.5	109.7	17.6	0.0273–5890	13.9	105.7	20.6
Zoghi and Shokouhi [22]	28–1361	24.2	42.4	26.2	14–1361	14.4	32.1	16.4	14–1361	20.4	36.5	22.2
Maddox et al. [27]	13.23–1536.6	−4.9	74.8	15.2	13.23–1536.6	−8.5	78.0	13.4	13.23–1536.6	−6.4	77.1	13.9
Huttenhuis et al. [25]	–	–	–	–	–	–	–	–	0.141–1.495	−35.0	0.3	35.0
Dicko et al. [29]	–	–	–	–	–	–	–	–	3–278	−17.0	11.6	17.0
Sadegh et al. [30]	–	–	–	–	–	–	–	–	53–386	−10.9	11.4	10.9
This work	–	–	–	–	–	–	–	–	2.60–818.12	−20.2	36.5	21.3
Overall		**0.9**	**70.4**	**30.4**		**3.5**	**66.2**	**17.8**		**5.1**	**58.4**	**20.6**
						Total pressure, P_{tot}						
Kuranov et al. [17]	165.2–4895.9	−9.6	240.3	12.5	165.2–4895.9	−10.5	241.1	13.6	165.2–4895.9	−10.0	241.5	12.9
Kamps et al. [18]	147.9–2783	−15.2	213.7	16.0	147.9–2783	−20.8	231.5	20.8	147.9–2783	−13.7	173.5	14.2
Sidi-Boumedine et al. [19]	6.21–1040	−10.8	55.4	12.6	6.21–1040	−16.4	70.3	16.7	6.21–1040	−9.9	56.2	11.0
Overall		**−11.0**	**194.4**	**13.2**		**−13.9**	**202.9**	**15.8**		**−10.8**	**187.9**	**12.7**

[a] $\text{BIAS}\ (\%) = \frac{1}{N}\sum \frac{P_s^{pred} - P_s^{exp}}{P_s^{exp}} \cdot 100,$

[b] $\text{AAD} = \frac{1}{N}\sum \left| P_s^{pred} - P_s^{exp} \right|,$

[c] $\text{AARD}\ (\%) = \frac{1}{N}\sum \left| \frac{P_s^{pred} - P_s^{exp}}{P_s^{exp}} \right| \cdot 100$

the data from Kim et al. [33] which are slightly higher than the data obtained on the same conditions by Daubert et al. [40] as well as our measurements. However, including those data leads to modelled vapor pressures with only the slightly higher AARD of 5%.

High-pressure VLE. The parameter fitting for the MDEA-H_2O system returned satisfactory AARDs for all three variables fitted, i.e. VLE (P_{tot}), FPD and H^E, as described in Sections 2.2 and 4. The calculated AARDs for each variable are shown in Table 12.

The model can predict very well the total pressure of the binary system, as witnessed above by the low AARD. The excess enthalpy H^E can be well predicted at temperatures of 298.15 and 313.15 K, though the model yields lower excess enthalpies at 338.15 K for MDEA concentrations lower than 85 wt%. At this temperature, the model was fitted to experimental data reported by Maham et al. [38] which shows the highest AARD. The corresponding figures for the total pressure, excess enthalpy and the freezing point depression are presented in Section C of Supplementary Information.

The fixed parameters in Table 7 and the regressed parameters for the binary subsystem MDEA-H_2O (Supplementary Information) were used for the regression of the ternary system H_2S-MDEA-H_2O. Initially, all the data from Table 1 were used for the parametrization of the model, except for the data from Li and Shen, as well as the data in the presence of methane (Case A). The data obtained in the presence of nitrogen were all included. The scatter already discussed earlier at low loadings resulted in high AARD, especially for the data points reported in terms of partial pressure of H_2S. The high deviations are also attributed to the much lower values of partial pressures in comparison with total ones, leading to higher relative numbers. Therefore, we have decided to also perform the data regression excluding all data at loadings lower than 0.05 mol H_2S/mol MDEA (Case B). This indeed improved substantially the fitting of the partial pressures, as one can see in the AARDs in Table 13, from approximately 30%–18%. The parity plot for the predicted and experimental values is shown in Fig. 8 while Fig. 9 shows the difference between predicted and experimental H_2S partial pressure as a function of the experimental value.

Significant scatter can be seen in the plots above at the lower pressures. At pressures P < 1 kPa, the model underestimates the data from Lemoine et al. [28] while overestimating the data from Jou et al. [12] and MacGregor and Mather [14]. The accuracy of the model is good for the data from Rogers et al. [24] and Jou et al. [21], with some data being underpredicted. The visual observations are depicted on the bias and AARD (%) calculations presented in Table 13. The negative bias whose absolute value is the same as the AARD for Lemoine et al.'s work shows that all data have been underestimated by the model. In addition, the fact that the AAD for this source is 0.2 kPa shows that the high AARD of 27% is due to the low values in partial pressures. At intermediate pressures, the scatter is less pronounced, but still the model overpredicts the data of MacGregor and Mather [14] and Jou et al. [12]. The BIAS and AARDs for these two are −37% and 38% and −27% and 27% respectively, while the rest of the sources show AARDs lower than 17%. At higher pressures, both Figs. 8 and 9 show that the model can predict well the literature data.

Overall, maximum AARD was found for the data from MacGregor and Mather [14] showing an almost 50% AARD in Case A and 38% in Case B. The minimum deviations observed were for the data from Maddox et al. [27] in Case A (13%) and from Huang and Ng [23] in Case B (9%). From the three experimental sets of total pressure, the one reported by Kuranov et al. showed the lowest deviations for both cases. Similar observations were made also by Huttenhuis et al. [20] during the evaluation of their model developed for the H2S-MDEA-H2O system. Although the model framework they used (electrolyte EoS for both phases) differs from ours, their model predictions also showed highest deviations for the data from MacGregor and Mather and lowest for the data from Maddox et al. [27] and Kuranov et al. [17]. Fig. 10 shows experimental and modelled values for a 50 wt% aqueous MDEA system as a function of temperature in Case B.

The differences in H_2S partial pressure noticed in the literature

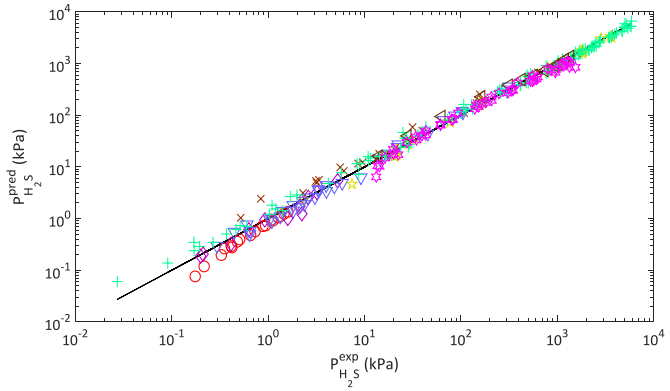

Fig. 8. Parity plot for different literature sources; ○ Lemoine et al. [28], □ Huang and Ng [23], ◊ Rogers et al. [24], × (MacGregor and Mather [14], ▽ Jou et al. [21], + Jou et al. [12], □ Zoghi and Shokouhi [22], □ Maddox et al. [27], (−) y = x.

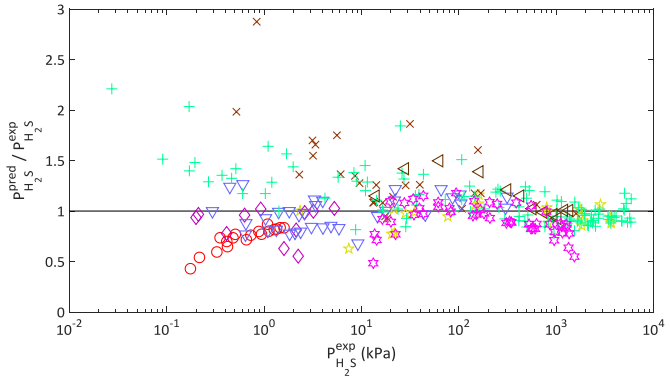

Fig. 9. Difference between predicted and experimental H_2S partial pressure as a function of the experimental value. ○ Lemoine et al. [28], □ Huang and Ng [23], ◊ Rogers et al. [24], × MacGregor and Mather [14], ▽ Jou et al. [21], + Jou et al. [12], □ Zoghi and Shokouhi [22], □ Maddox et al. [27].

data as well as in our data obtained in the presence of methane for relatively low total pressure levels, are comparable to the accuracy of the model. Therefore, since also the effect of methane in the liquid loading has been found to be negligible for a 70 wt% MDEA-H_2O, we also fitted the model to data available in the presence of methane. However, the code was not modified but, instead, the data for partial pressure of H_2S and loading were used as if methane

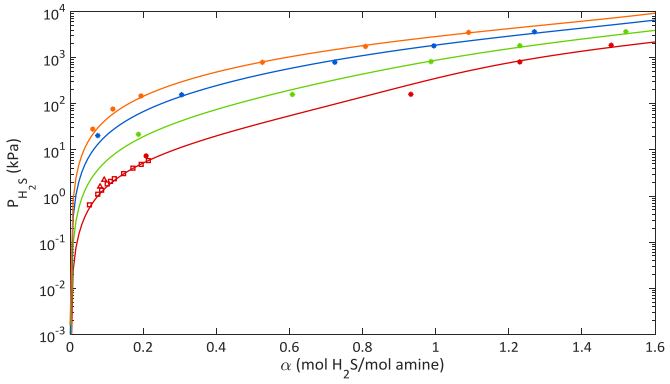

Fig. 10. Hydrogen sulfide loading for 50 wt% MDEA-H_2O as a function of partial pressure and temperature; (red) 313 K, (green) 343 K, (blue) 373 K, (orange) 393 K; (−) model, * Huang and Ng [23], Δ Rogers et al. [24] (1998), □ Jou et al. [21] (1993). Regression in Case B.

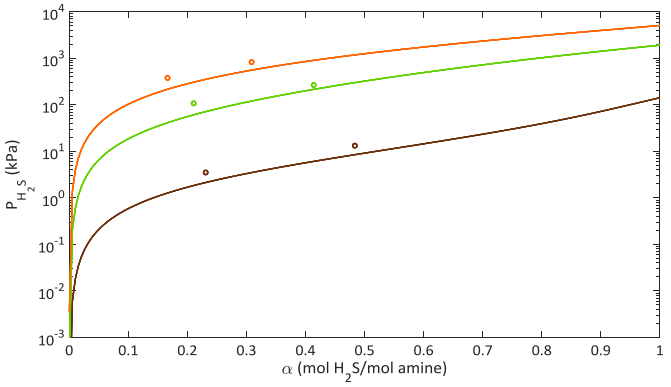

Fig. 11. Hydrogen sulfide loading for 70 wt% MDEA-H_2O as a function of partial pressure and temperature; (brown) 283 K, (green) 353 K, (orange) 393 K; (−) model, ○ This work. Regression in Case C.

was not present. Only data with maximum total pressure of 2000 kPa were considered, due to the more significant P_{H2S} deviations observed at higher pressures in the literature for a 50 wt% aqueous MDEA (Case C). To sum up, three cases were studied:

Case A. Regression of all available data in the absence of methane.
Case B. Regression of all available data in the absence of methane and loadings $\alpha > 0.05$ mol H_2S/mol MDEA.
Case C. Regression of all available data in the absence of methane and loadings $\alpha > 0.05$ mol H_2S/mol MDEA, and the data in the presence of methane, loadings $\alpha > 0.05$ mol H_2S/mol MDEA and maximum total pressures P_{tot} of 2000 kPa.

The model parameters obtained from the data regression in each case studied are given in Supplementary Information. Fig. 11 shows experimental and modelled values for a 70 wt% aqueous MDEA system as a function of temperature in Case C while Table 13 contains information about each regression in terms of Bias, AADs and AARDs. The performance of the model for a 70 wt% MDEA-H_2O system is good, especially considering the few data available for this solvent concentration. In Table 13, it can be seen that the accuracy of the model does not significantly change upon the addition of the experimental points with methane in the regression. The overall AARD for the partial pressure is altered from 18% to 21%, which is also the AARD calculated for the data published in this work. The data from MacGregor and Mather [14] exhibit again the highest deviations while the measurements reported by Sadegh et al. [30]

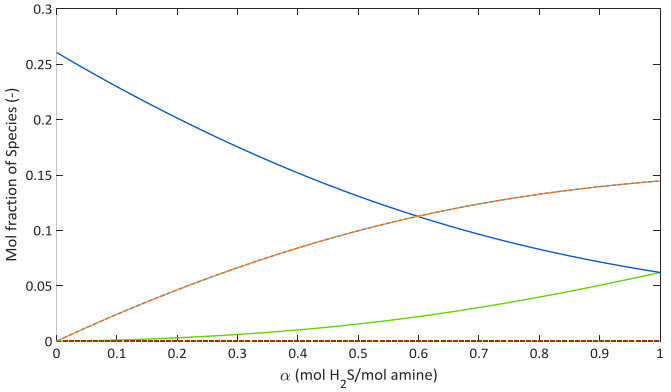

Fig. 12. Predicted speciation of H_2S, MDEA and H_2O in 70 wt% MDEA-H_2O at 353 K. (—) H_2S, (—) MDEA, (—) H_2O, (—) $MDEAH^+$, (- -) OH^-, (- -) HS^-.

in total pressure of 1500 kPa with methane as makeup gas show the lowest deviation, 11%. The slight deterioration of the fitting for the equilibrium H_2S can be also attributed to the fact that experimental points obtained for high amine concentrations are used, i.e. 70 wt% in this work, but it can also be the result of the sensitivity of the algorithm to the numerical method. To illustrate the latter, we repeated the data regression for Case A. The resulted AARDs were 29.8% and 30.1%, using the exact same data and fixed parameters. As far as the ability of the model to predict the total pressure is concerned, the accuracy has surprisingly improved. This is merely a lucky coincidence due to the fitting of the experimental points for methane-included systems.

Speciation information is necessary in the development of process models for the accurate design and operation of gas processing plants. Speciation results, calculated with the model presented in this work, are provided in Fig. 12 where mole fractions of all the species in the liquid phase are plotted against liquid loading for 70 wt% aqueous MDEA at 353 K. It is shown that as the loading increases, the concentration of MDEA declines and the concentration of protonated amine $MDEAH^+$ increases. At loadings close to 1, most of the amine has been protonated and the mole fractions of MDEA and H_2S are equal. The curves representing $MDEAH^+$ and HS^- overlap, a behavior expected since the formation of sulfide was not taken into account due to its low concentration, therefore the amount of HS^- and $MDEAH^+$ formed are balanced. H_3O^+ and OH^- also overlap and they are practically zero throughout the loading range. No experimental data were found for the speciation distribution in the H_2S-MDEA-H_2O system to confirm the model predictions. Speciation graphs for 50.1 wt% and 70 wt% MDEA-H_2O at the temperatures studied in this work are provided in Supplementary Information.

Overall, although the model developed in this work contains MDEA, H_2O, H_2S and the relevant ionic species, it can predict vapor-liquid equilibria for systems containing methane at low total pressures with similar accuracy as the systems in the absence of methane. However, it is recommended to be used only for rough estimations for H_2S–CH_4-MDEA-H_2O system and a model taking into account the methane solubility to be used if available. This model should not be used for systems with total pressure higher than 2000 kPa, where the gas fugacities change substantially.

6. Conclusions

Experimental vapor-liquid equilibrium data were measured for a 50.1 wt% aqueous MDEA at temperature of 323 K and pressure up to 3000 kPa as well as a 70 wt% aqueous MDEA at temperature of 283 K, 353 K and 323 K and pressures up to 10000 kPa, due to their relevance for subsea H_2S removal of natural gas. Therefore, methane was used as makeup gas. The experimental data indicate that the effect of total pressure on the liquid loading of the solvent is within the experimental uncertainties, while for the 50 wt% MDEA-H_2O system the impact on the partial pressure of hydrogen sulfide is attributed to the non-idealities of the vapor phase and it is lower with decreasing total pressure. The system H_2S-MDEA-H_2O up to 70 wt% MDEA was modelled employing Peng-Robinson EoS to describe the vapor phase and eNRTL activity coefficient model for the liquid phase. The AARD for the partial pressure of H_2S and for the total system pressure was found to be 18% and 16% respectively. The effect of including data in the presence of methane and maximum total pressure of 2000 kPa in the data regression was studied and found minimal. However, for higher total pressure and different conditions than the studied ones, the use of models taking into account the methane presence was suggested. Last but not least, new parameters for Antoine correlation were proposed for the estimation of the vapor pressure of MDEA based on our new measurements and all available literature data covering a wide temperature range.

Funding

This work was supported by the Norwegian University of Science and Technology (NTNU), major industry partners and the Research Council of Norway (RCN) [project number 237893]. It was carried out as a part of SUBPRO (Subsea Production and Processing), a Research-based Innovation Centre within Subsea Production and Processing.

Declaration of competing interest

The authors declare that they have no known competing financial interests or personal relationships that could have appeared to influence the work reported in this paper.

CRediT authorship contribution statement

Eirini Skylogianni: Conceptualization, Investigation, Software, Validation, Writing - original draft, Writing - review & editing. **Ingvild Mundal:** Investigation, Software. **Diego D.D. Pinto:** Conceptualization, Investigation, Software, Writing - review & editing, Supervision, Project administration. **Christophe Coquelet:** Investigation, Writing - review & editing, Supervision. **Hanna K. Knuutila:** Conceptualization, Investigation, Writing - review & editing, Supervision, Project administration, Funding acquisition.

Acknowledgements

The authors acknowledge the valuable help from Mr. Eric Boonaert and Ing. Alain Valtz during the laboratory work with the high-pressure VLE apparatus. Anastasia A. Trollebø is acknowledged for conducting the pure MDEA saturation pressure measurements and Ricardo R. Wanderley for the insightful discussions.

List of Symbols

Latin letters

a	parameter of Eq. 10
A_Φ	Debye-Hückel parameter
b	parameter of Eq. 10
c-a	cation-anion
D	Dielectric constant (−)
g^{ex}	Molar excess Gibbs energy (J/mol)
G	eNRTL auxiliary function (−)
H	Henry's constant (kPa m^3/kmol)
I_x	Ionic strength in mole fraction scale (mol/m^3)
k	Boltzmann constant (J/K)
m	molecule
M	Molecular weight (kg/kmol)
N_A	Avogadro number (mol^{-1})
P	Pressure (kPa)
r_{BORN}	Born radius (m)
R	Gas constant (J mol^{-1} K^{-1})
T	Absolute temperature (K)
v	Molar volume (m^3/mol)
w	Weight fraction (−)
x	Mole fraction (−)
X	eNRTL mole fraction (−)
z	Ionic charge (−)
Z	Absolute value of the ionic charge (−)

Greek letters

α	Loading (mol H_2S/mol MDEA)
γ	Activity coefficient (−)
ε	Permittivity (F/m)
ρ	Molar density (mol/cm^3)
ρ_{pdh}	Closest approach parameter of the Pitzer-Debye-Hückel formulation (−)
τ	Energy parameter (−)

Superscripts

E	Excess property
exp	Experimental value
l	Liquid phase
lc	Local composition
pdh	Pitzer-Debye-Hückel formulation
pred	Predicted value
v	Vapor phase

Subscripts

amb	Ambient
c	Critical
glob	Global, refers to global loading α_{glob} (mol H_2S in the cell/ mol MDEA)
i, j, k	Component in a mixture
ij	Cross parameter
liq	Liquid, refers to liquid loading α_{liq} (mol H_2S/mol MDEA)
s	solvent
w	water

Abbreviations

AAD	Average Absolute Deviation
AARD	Average Absolute Relative Deviation
eNRTL	electrolyte Non-Random Two Liquids
EoS	Equation of State
FPD	Freezing Point Depression
FTIR	Fourier-Transform infrared
GC	Gas Chromatography
MDEA	Methyldiethanolamine
NP	Number of data points
NS	Number of vapor phase samples for GC analysis
VLE	Vapor-Liquid Equilibrium

Appendix A. eNRTL model

The activity coefficients were calculated by the electrolyte Non-Random Two Liquids (eNRTL) model [50]. The starting point for the description of the liquid phase is the expression of excess Gibbs energy as the sum of two terms; one related to the long-range forces between the ions (first term) and one to the short-range forces between all the species (second term):

$$\frac{g^E}{RT}=\frac{g^{E,pdh}}{RT}+\frac{g^{E,\,lc}}{RT} \tag{A1}$$

This equation lead to:

$$\ln\gamma_i=\ln\gamma_i^{pdh}+\ln\gamma_i^{lc} \tag{A2}$$

The subscript *pdh* denotes Pitzer-Debye-Hückel formulation for the long-range interactions and the subscript *lc* denotes Local Composition model. The formulation of the former is:

$$\frac{g^{E,pdh}}{RT}=-\left(\sum_k x_k\right)\left(\frac{1000}{M_s}\right)^{\frac{1}{2}}\left(\frac{4A_\Phi I_x}{\rho_{pdh}}\right)\ln\left(1+\rho_{pdh}I_x^{\frac{1}{2}}\right) \tag{A3}$$

By derivation, the activity coefficient is expressed according to:

$$\ln\gamma_i^{*pdh}=-(1000/M_s)^{\frac{1}{2}}A_\Phi\left[\times\left(2\frac{Z_i^2}{\rho_{pdh}}\right)\ln\left(1+\rho_{pdh}I_x^{\frac{1}{2}}\right)+\left(Z_i^2I_x^{\frac{1}{2}}-2\,I_x^{\frac{3}{2}}\right)\Big/\left(1+\rho_{pdh}\,I_x^{\frac{1}{2}}\right)\right] \tag{A4}$$

where I_x is the ionic strength and A_Φ is the Debye-Hückel parameter, expressed as following:

$$I_x=\frac{1}{2}\sum_i Z_i^2x_i \tag{A5}$$

$$A_\Phi=\frac{1}{3}\left(\frac{2\pi N_o d}{1000}\right)^{\frac{1}{2}}\left(\frac{e^2}{DkT}\right)^{3/2} \tag{A6}$$

The reference state for the *pdh* term is infinite dilution in the mixed solvent while the reference state for the *lc* term is infinite dilution in water. To account for the excess Gibbs energy of transfer from the infinite dilution in the mixed solvent to the infinite dilution in water, a term is added in the long-range interaction expression. This additional term is described by the Born equation:

$$\frac{g^{E,BORN}}{RT}=-\frac{N_Ae^2}{8\pi RTr_{BORN}\varepsilon_o}\left(\frac{1}{\varepsilon_s}-\frac{1}{\varepsilon_w}\right)\sum_i x_iz_i^2 \tag{A7}$$

Further,

$$\ln\gamma_i^{BORN}=\frac{N_Ae^2}{8\pi RTr_{BORN}\varepsilon_o}\left(\frac{1}{\varepsilon_s}-\frac{1}{\varepsilon_w}\right)z_i^2 \tag{A8}$$

The short-range contribution is described by the eNRTL model as following:

$$\frac{g^{E,\,lc}}{RT}=\sum_m X_m\frac{\sum_j X_jG_{jm}\tau_{jm}}{\sum_k X_kG_{km}}+\sum_c X_c\sum_{a'}\frac{X_{a'}}{\sum_k X_kG_{km}}\frac{\sum_j X_jG_{jc,a'c}\tau_{jc,a'c}}{\sum_k X_kG_{kc,a'c}}+\sum_a X_a\sum_{c'}\frac{X_{c'}}{\sum_{c''}X_{c''}}\frac{\sum_j X_jG_{ja,c'a}\tau_{ja,c'a}}{\sum_k X_kG_{ka,c'a}} \tag{A9}$$

where m, c and a denote molecule, cation and anion, while $X_j = C_jx_j$ with j: m, c, a effective local mole fraction. Equations A10 and A11 are given using the ion-like repulsion assumption and the local electroneutrality assumption.

$$G_{cm}=\frac{\sum_a X_aG_{ca,\,m}}{\sum_{a'}X_{a'}} \tag{A10}$$

$$G_{am}=\frac{\sum_c X_cG_{ca,\,m}}{\sum_{c'}X_{c'}} \tag{A11}$$

The $G_{i,j}$ and $\tau_{i,j}$ parameters are related through the non-randomness parameter, $a_{i,j}$:

$$G_{ij} = \exp(-a_{i,j}\tau_{i,j}) \quad \text{A12}$$

The equations presented below describe the non-randomness parameters:

$$a_{cm} = \frac{\sum_a X_a a_{ca,\,m}}{\sum_{a'} X_{a'}} \quad \text{A13}$$

$$a_{am} = \frac{\sum_c X_c a_{ca,\,m}}{\sum_{c'} X_{c'}} \quad \text{A14}$$

The energy parameters $\tau_{mc,\,ac}$ and $\tau_{ma,\,ca}$ are given by:

$$\tau_{mc,\,ac} = \tau_{cm} - \frac{a_{ca,m}}{a_{mc,ac}}\left(\tau_{ca,m} - \tau_{m,ca}\right) \quad \text{A15}$$

$$\tau_{ma,\,ca} = \tau_{am} - \frac{a_{ca,m}}{a_{ma,ac}}\left(\tau_{ca,m} - \tau_{m,ca}\right) \quad \text{A16}$$

where $a_{mc,ac} = a_{cm}$ and $a_{am,ac} = a_{am}$.The adjustable binary parameters are the non-randomness factors $a_{ca,m}$, $a_{ca,ca'}$, $a_{ca,c'a}$, $a_{mm'}$, and the energy parameters $\tau_{ca,m}$, $\tau_{m,ca}$, $\tau_{ca,ca'}$, $\tau_{ca',ca}$, $\tau_{ca,c'a}$, $\tau_{c'a,ca}$, $\tau_{m,m'}$, $\tau_{m'm}$.

From Equation (A9), the activity coefficients are calculated:

For molecules:

$$\ln\gamma_m^{lc} = \frac{\sum_j X_j G_{jm}\tau_{jm}}{\sum_k X_k G_{km}} + \sum_{m'}\frac{X_{m'}G_{mm'}}{\sum_k X_k G_{km'}}\left(\tau_{mm'} - \frac{\sum_k X_k G_{km'}\tau_{km'}}{\sum_k X_k G_{km'}}\right) + \sum_c\sum_{a'}\frac{X_{a'}}{\sum_{a''}X_{a''}}\frac{X_{c'}G_{mc,a'c}}{\sum_k X_k G_{kc,a'c}}\left(\tau_{mc,a'c} - \frac{\sum_k X_k G_{kc,a'c}\tau_{kc,a'c}}{\sum_k X_k G_{kc,a'c}}\right) + \sum_a\sum_{c'}\frac{X_{c'}}{\sum_{c''}X_{c''}}\frac{X_{a'}G_{ma,c'a}}{\sum_k X_k G_{ka,c'a}}\left(\tau_{ma,c'a} - \frac{\sum_k X_k G_{ka,c'a}\tau_{ka,c'a}}{\sum_k X_k G_{ka,c'a}}\right) \quad \text{A17}$$

For cations:

$$\frac{1}{Z_c}\ln\gamma_c^{lc} = \sum_{a'}\frac{X_{a'}}{\sum_{a''}X_{a''}}\frac{\sum_k X_k G_{kc,\,a'c}\tau_{kc,a'c}}{\sum_k X_k G_{kc,a'c}} + \sum_m\frac{X_m G_{cm}}{\sum_k X_k G_{km}}\left(\tau_{cm} - \frac{\sum_k X_k G_{km}\tau_{km}}{\sum_k X_k G_{km}}\right) + \sum_a\sum_{c'}\frac{X_{c'}}{\sum_{c''}X_{c''}}\frac{X_{a'}G_{ca,c'a}}{\sum_k X_k G_{ka,c'a}}\left(\tau_{ca,c'a} - \frac{\sum_k X_k G_{ka,c'a}\tau_{ka,c'a}}{\sum_k X_k G_{ka,c'a}}\right) \quad \text{A18}$$

For anions:

$$\frac{1}{Z_a}\ln\gamma_a^{lc} = \sum_{c'}\frac{X_{c'}}{\sum_{c''}X_{c''}}\frac{\sum_k X_k G_{ka,\,c'a}\tau_{ka,\,c'a}}{\sum_k X_k G_{ka,\,c'a}} + \sum_m\frac{X_m G_{am}}{\sum_k X_k G_{km}}\left(\tau_{am} - \frac{\sum_k X_k G_{km}\tau_{km}}{\sum_k X_k G_{km}}\right) + \sum_c\sum_{a'}\frac{X_{a'}}{\sum_{a''}X_{a''}}\frac{X_c G_{ac,a'c}}{\sum_k X_k G_{kc,a'c}}\left(\tau_{ac,a'c} - \frac{\sum_k X_k G_{kc,a'c}\tau_{kc,a'c}}{\sum_k X_k G_{kc,a'c}}\right) \quad \text{A19}$$

The expressions of activity coefficients at infinite dilution are then:

$$\ln\gamma_m^{lc,\infty} = \tau_{wm} + G_{mw}\tau_{mw} \quad \text{A20}$$

$$\frac{1}{Z_c}\ln\gamma_c^{lc,\infty} = \frac{X_a}{\sum_{a'}X_{a'}}\tau_{wc,ac} + G_{cw}\tau_{cw} \quad \text{A21}$$

$$\frac{1}{Z_a}\ln\gamma_a^{lc,\infty} = \frac{X_c}{\sum_{c'}X_{c'}}\tau_{wa,ca} + G_{aw}\tau_{aw} \quad \text{A22}$$

By combination of Equations (A2), A4, A7, A18 and A23, the activity coefficient for the liquid phase is found by:

$$\gamma_\iota = \gamma_i^{pdh}\,\gamma_i^{BORN}\gamma_i^{lc}\Big/\gamma_i^{lc,\infty} \quad \text{A23}$$

where $i = m$, c or a for all components, besides the amine in this work. For MDEA, the symmetric reference state for the short-range interactions contribution, $\gamma_{MDEA}^{lc,\infty}$ is fixed to 1.

Appendix B. Peng-Robinson Equation of State

The fugacity coefficients were calculated by Peng-Robinson equation of state [49]:

$$P = \frac{RT}{v-b} - \frac{\alpha\ \mathrm{a}(T)}{v^2 + 2bv - b^2} \quad \text{A24}$$

where:

$$a = 0.42724\frac{R^2T_c^2}{P_c} \quad \text{A25}$$

$$b = 0.07780\frac{RT_c}{P_c}, \quad \mathrm{a}(T) = \left[1 + m\left(1 - T_R^{\frac{1}{2}}\right)\right]^2 \quad \text{A26}$$

$$m = 0.37464 + 1.54226\omega - 2.26992\omega^2 \quad \text{A27}$$

The traditional van der Waals one-fluid mixing rules were used for the estimation of the gas mixture parameters from the pure components' properties.

$$a\ \mathrm{a}(T) = \sum_i\sum_j x_i x_j (a\mathrm{a}(T))_i^{\frac{1}{2}}(a\mathrm{a}(T))_j^{\frac{1}{2}}(1 - k_{ij}) \quad \text{A28}$$

$$b = \sum_i x_i b_i \quad \text{A29}$$

In our work, the binary interaction parameter k_{ij} is set to zero, so as the eNRTL model parameters are the only ones fitted.

The critical properties used in this work can be found in Supplementary Information.

Appendix C. Supplementary data

Supplementary data to this article can be found online at https://doi.org/10.1016/j.fluid.2020.112498.

References

[1] G. Astarita, D.W. Savage, A. Bisio, Gas Treating with Chemical Solvents, John Wiley, New York, United States, 1983.
[2] J.M. Campbell, Amine-based processes, in: Gas Conditioning And Processing, vol. 4, 1998. Oklahoma, USA.

[3] A.L. Kohl, R.B. Nielsen, Chapter 2 - alkanolamines for hydrogen sulfide and carbon dioxide removal, in: Gas Purification, fifth ed., Gulf Professional Publishing, Houston, 1997, pp. 40–186.

[4] Z.I. Khatib, J.R. Salanitro, Reservoir souring: analysis of surveys and experience in sour waterfloods, in: Presented at the SPE Annual Technical Conference and Exhibition, 1997, https://doi.org/10.2118/38795-MS.

[5] A. F. Mitchell and S. Asa, "10248: A REVIEW OF RESERVOIR SOURING FOR THREE NORTH SEA FIELDS.," p. 8.

[6] GATEkeeper, H2S Scavenging: Using Triazine, May-2014.

[7] O. Økland, S. Davies, R.M. Ramberg, H. Rognø, "Steps to the Subsea Factory," in *OTC-24307-MS*, OTC, 2013, https://doi.org/10.4043/24307-MS.

[8] M. Davoudi, Y. Heidari, A. Safadoost, S. Samieirad, Chemical injection policy for internal corrosion prevention of South Pars sea-pipeline: a case study, J. Nat. Gas Sci. Eng. 21 (Nov. 2014) 592–599, https://doi.org/10.1016/j.jngse.2014.09.017.

[9] UWP/Subsea on a Stick®," *kvaerner - UWP/Subsea on a Stick®* [Online]. Available, https://www.kvaerner.com/Products/Subsea-on-a-Stick/. (Accessed 13 March 2019).

[10] J. Addicks, G.A. Owren, A.O. Fredheim, K. Tangvik, Solubility of carbon dioxide and methane in aqueous methyldiethanolamine solutions, J. Chem. Eng. Data 47 (4) (Jul. 2002) 855–860, https://doi.org/10.1021/je010292z.

[11] Ø. Jonassen, Equilibrium and Thermal Properties of Selected CO2-methane-tertiary Amine Systems; an Experimental and Modelling Study, NTNU, 2017.

[12] F.Y. Jou, A.E. Mather, F.D. Otto, Solubility of hydrogen sulfide and carbon dioxide in aqueous methyldiethanolamine solutions, Ind. Eng. Chem. Process Des. Dev. 21 (4) (Oct. 1982) 539–544, https://doi.org/10.1021/i200019a001.

[13] M.H. Li, K.P. Shen, Solubility of hydrogen sulfide in aqueous mixtures of monoethanolamine with N-methyldiethanolamine, J. Chem. Eng. Data 38 (1) (Jan. 1993) 105–108, https://doi.org/10.1021/je00009a025.

[14] R.J. MacGregor, A.E. Mather, Equilibrium solubility of H2S and CO2 and their mixtures in a mixed solvent, Can. J. Chem. Eng. 69 (6) (Dec. 1991) 1357–1366, https://doi.org/10.1002/cjce.5450690618.

[15] J.M. Bernal-García, M. Ramos-Estrada, G.A. Iglesias-Silva, K.R. Hall, Densities and excess molar volumes of aqueous solutions of n-methyldiethanolamine (MDEA) at temperatures from (283.15 to 363.15) K, J. Chem. Eng. Data 48 (6) (Nov. 2003) 1442–1445, https://doi.org/10.1021/je030120x.

[16] L. Chunxi, W. Fürst, Representation of CO2 and H2S solubility in aqueous MDEA solutions using an electrolyte equation of state, Chem. Eng. Sci. 55 (15) (Aug. 2000) 2975–2988, https://doi.org/10.1016/S0009-2509(99)00550-3.

[17] G. Kuranov, B. Rumpf, N.A. Smirnova, G. Maurer, "Solubility of single gases carbon dioxide and hydrogen sulfide in aqueous solutions of N-methyldiethanolamine in the temperature range 313–413 K at pressures up to 5 MPa, Ind. Eng. Chem. Res. 35 (6) (Jan. 1996) 1959–1966, https://doi.org/10.1021/ie950538r.

[18] Á.P.-S. Kamps, A. Balaban, M. Jödecke, G. Kuranov, N.A. Smirnova, G. Maurer, "Solubility of single gases carbon dioxide and hydrogen sulfide in aqueous solutions of N-methyldiethanolamine at temperatures from 313 to 393 K and pressures up to 7.6 MPa: new experimental data and model extension, Ind. Eng. Chem. Res. 40 (2) (Jan. 2001) 696–706, https://doi.org/10.1021/ie000441r.

[19] R. Sidi-Boumedine, S. Horstmann, K. Fischer, E. Provost, W. Fürst, J. Gmehling, Experimental determination of hydrogen sulfide solubility data in aqueous alkanolamine solutions, Fluid Phase Equil. 218 (1) (Apr. 2004) 149–155, https://doi.org/10.1016/j.fluid.2003.11.020.

[20] P.J.G. Huttenhuis, N.J. Agrawal, G.F. Versteeg, The solubility of hydrogen sulfide in aqueous N-methyldiethanolamine solutions, Int. J. Oil Gas Coal Technol. 1 (4) (2008) 399–424.

[21] F.-Y. Jou, J.J. Carroll, A.E. Mather, F.D. Otto, The solubility of carbon dioxide and hydrogen sulfide in a 35 wt% aqueous solution of methyldiethanolamine, Can. J. Chem. Eng. 71 (2) (Apr. 1993) 264–268, https://doi.org/10.1002/cjce.5450710213.

[22] A.T. Zoghi, M. Shokouhi, Measuring solubility of hydrogen sulphide in aqueous blends of N-methyldiethanolamine and 2-((2 aminoethyl)amino) ethanol and correlating by the Deshmukh-Mather model, J. Chem. Thermodyn. 100 (2016) 106–115, https://doi.org/10.1016/j.jct.2016.04.012.

[23] S.H. Huang, H.-J. Ng, Solubility of H2S and CO2 in Alkanolamines, Gas Processors Association, Sep. 1998. RR-155.

[24] W.J. Rogers, J.A. Bullin, R.R. Davison, FTIR measurements of acid-gas - methyldiethanolamine systems, AIChE J. 44 (11) (1998) 2423–2430.

[25] P.J.G. Huttenhuis, N.J. Agrawal, J.A. Hogendoorn, G.F. Versteeg, Gas solubility of H2S and CO2 in aqueous solutions of N-methyldiethanolamine, J. Petrol. Sci. Eng. 55 (1) (Jan. 2007) 122–134, https://doi.org/10.1016/j.petrol.2006.04.018.

[26] A.M. Bhairi, Experimental Equilibrium between Acid Gases and Ethanolamine Solutions, Jul. 1984.

[27] R.N. Maddox, A.H. Bhairi, J.R. Diers, P.A. Thomas, Equilibrium Solubility of Carbon Dioxide or Hydrogen Sulfide in Aqueous Solutions of Monoethanolamine, Diglycolamine, Diethanolamine and Methyldiethanolamine: Project 841 vol. 104, Gas Processors Association, Tulsa, Okla, RR-, 1987.

[28] B. Lemoine, Y.-G. Li, R. Cadours, C. Bouallou, D. Richon, Partial vapor pressure of CO2 and H2S over aqueous methyldiethanolamine solutions, Fluid Phase Equil. 172 (2) (Jul. 2000) 261–277, https://doi.org/10.1016/S0378-3812(00)00383-6.

[29] M. Dicko, C. Coquelet, C. Jarne, S. Northrop, D. Richon, Acid gases partial pressures above a 50 wt% aqueous methyldiethanolamine solution: experimental work and modeling, Fluid Phase Equil. 289 (2) (Mar. 2010) 99–109, https://doi.org/10.1016/j.fluid.2009.11.012.

[30] N. Sadegh, K. Thomsen, E. Solbraa, E. Johannessen, G.I. Rudolfsen, O.J. Berg, Solubility of hydrogen sulfide in aqueous solutions of N-methyldiethanolamine at high pressures, Fluid Phase Equil. 393 (May 2015) 33–39, https://doi.org/10.1016/j.fluid.2015.02.016.

[31] H.T. Chang, M. Posey, G.T. Rochelle, Thermodynamics of alkanolamine-water solutions from freezing point measurements, Ind. Eng. Chem. Res. 32 (10) (1993) 2324–2335.

[32] P.L. Fosbøl, M.G. Pedersen, K. Thomsen, "Freezing point depressions of aqueous MEA, MDEA, and MEA–MDEA measured with a new apparatus, J. Chem. Eng. Data 56 (4) (Apr. 2011) 995–1000, https://doi.org/10.1021/je100994v.

[33] I. Kim, H.F. Svendsen, E. Børresen, "Ebulliometric determination of Vapor–Liquid equilibria for pure water, monoethanolamine, N-methyldiethanolamine, 3-(Methylamino)-propylamine, and their binary and ternary solutions, J. Chem. Eng. Data 53 (11) (Nov. 2008) 2521–2531, https://doi.org/10.1021/je800290k.

[34] S. Xu, S. Qing, Z. Zhen, C. Zhang, J.J. Carroll, Vapor pressure measurements of aqueous N-methyldiethanolamine solutions, Fluid Phase Equil. 67 (Nov. 1991) 197–201, https://doi.org/10.1016/0378-3812(91)90055-C.

[35] E. Voutsas, A. Vrachnos, K. Magoulas, Measurement and thermodynamic modeling of the phase equilibrium of aqueous N-methyldiethanolamine solutions, Fluid Phase Equil. 224 (2) (Oct. 2004) 193–197, https://doi.org/10.1016/j.fluid.2004.05.012.

[36] M.L. Posey, Thermodynamic Model for Acid Gas Loaded Aqueous Alkanolamine Solutions, 1996.

[37] Y. Maham, A.E. Mather, L.G. Hepler, Excess molar enthalpies of (water + alkanolamine) systems and some thermodynamic calculations, J. Chem. Eng. Data 42 (5) (Sep. 1997) 988–992, https://doi.org/10.1021/je960296h.

[38] Y. Maham, A.E. Mather, C. Mathonat, Excess properties of (alkyldiethanolamine +H2O) mixtures at temperatures from (298.15 to 338.15) K, J. Chem. Therm. 32 (2) (Feb. 2000) 229–236, https://doi.org/10.1006/jcht.1999.0595.

[39] O. Noll, A. Valtz, D. Richon, T. Getachew-Sawaya, I. Mokbel, J. Jose, Vapor pressures and liquid densities of N-methylethanolamine, diethanolamine, and N-methyldiethanolamine, ELDATA: Int. Electron. J. Phys.-Chem. Data 4 (1998) 105–120.

[40] T.E. Daubert, J.W. Jalowka, V. Goren, Vapor pressure of 22 pure industrial chemicals, AICHE Symp. Ser. 83 (1987) 128–156.

[41] C. Yang, et al., "Vapor–Liquid equilibria for three binary systems of N-methylethanolamine, N-methyldiethanolamine, and ethylene glycol at P = (40.0, 30.0, and 20.0) kPa, J. Chem. Eng. Data 58 (8) (Aug. 2013) 2272–2279, https://doi.org/10.1021/je400373d.

[42] D.M. VonNiederhausern, G.M. Wilson, N.F. Giles, Critical point and vapor pressure measurements for 17 compounds by a low residence time flow method, J. Chem. Eng. Data 51 (6) (Nov. 2006) 1990–1995, https://doi.org/10.1021/je060269j.

[43] J.M.S. Fonseca, R. Dohrn, S. Peper, "High-pressure fluid-phase equilibria: experimental methods and systems investigated (2005–2008), Fluid Phase Equil. 300 (1) (Jan. 2011) 1–69, https://doi.org/10.1016/j.fluid.2010.09.017.

[44] ARMINES, Procédé et Dispositif Pour Prélever Des Microéchantillons D'un Fluide Sous Pression Contenu Dans Un Container 2 853 414 (2003).

[45] E.W. Lemmon, I.H. Bell, M.L. Huber, M.O. McLinden, NIST Standard Reference Database 23: Reference Fluid Thermodynamic and Transport Properties-REFPROP, National Institute of Standards and Technology, Standard Reference Data Program, Gaithersburg, 2018.

[46] E.W. Lemmon, R. Span, Short fundamental equations of state for 20 industrial fluids, J. Chem. Eng. Data 51 (3) (May 2006) 785–850, https://doi.org/10.1021/je050186n.

[47] J.G.M.-S. Monteiro, D.D.D. Pinto, S.A.H. Zaidy, A. Hartono, H.F. Svendsen, VLE data and modelling of aqueous N,N-diethylethanolamine (DEEA) solutions, Int. J. Greenh. Gas. Cntrl. 19 (Nov. 2013) 432–440, https://doi.org/10.1016/j.ijggc.2013.10.001.

[48] D.D.D. Pinto, J.G.M.-S. Monteiro, A. Bersås, T. Haug-Warberg, H.F. Svendsen, eNRTL parameter fitting procedure for blended amine systems: MDEA-PZ case study, Energy Procedia 37 (Jan. 2013) 1613–1620, https://doi.org/10.1016/j.egypro.2013.06.037.

[49] D.-Y. Peng, D.B. Robinson, A new two-constant equation of state, Ind. Eng. Chem. Fund. 15 (1) (Feb. 1976) 59–64, https://doi.org/10.1021/i160057a011.

[50] C.-C. Chen, L.B. Evans, A local composition model for the excess Gibbs energy of aqueous electrolyte systems, AIChE J. 32 (3) (1986) 444–454, https://doi.org/10.1002/aic.690320311.

[51] J.L. Oscarson, X. Chen, R.M. Izatt, A Thermodynamically Consistent Model for the Prediction of Solubilities and Enthalpies of Solution of Acid Gases in Aqueous Alkanolamine Solutions, Gas Processors Association, Tulsa, Oklahoma,, 1995. RR-130.

[52] T.J. Edwards, J. Newman, J.M. Prausnitz, Thermodynamics of vapor-liquid equilibria for the ammonia-water system, Ind. Eng. Chem. Fundam. 17 (4) (Nov. 1978) 264–269, https://doi.org/10.1021/i160068a007.

[53] DIPPR, DIPPR Chemical Database, Design Institute for Physical Property Data American Institute of Chemical Engineers, 2004.

[54] E.T. Hessen, T. Haug-Warberg, H.F. Svendsen, "The refined e-NRTL model applied to CO2–H2O–alkanolamine systems, Chem. Eng. Sci. 65 (11) (Jun. 2010) 3638–3648, https://doi.org/10.1016/j.ces.2010.03.010.

[55] J. Kennedy, R.C. Eberhart, Proceedings of IEEE International Conference on

Neural Networks, 1995. Perth, Australia.
[56] S. Ghosh, S. Das, D. Kundu, K. Suresh, A. Abraham, Inter-particle communication and search-dynamics of lbest particle swarm optimizers: an analysis, Inf. Sci. 182 (1) (Jan. 2012) 156–168, https://doi.org/10.1016/j.ins.2010.10.015.
[57] D.D.D. Pinto, CO2 Capture Solvents; Modeling and Experimental Characterization, Norwegian University of Science and Technology, 2014.
[58] B.N. Taylor, C.E. Kuyatt, NIST Guidelines for Evaluating and Expressing the Uncertainty of NIST Measurement Results. NIST Technical Note 1297." Physics Laboratory, National Institute of Standards and Technology, Sep-1994.
[59] E.B. Rinker, O.C. Sandall, Physical solubility of hydrogen sulfide in several aqueous solvents, Can. J. Chem. Eng. 78 (1) (Feb. 2000) 232–236, https://doi.org/10.1002/cjce.5450780130.
[60] H.A. Al-Ghawas, D.P. Hagewiesche, G. Ruiz-Ibanez, O.C. Sandall, Physicochemical properties important for carbon dioxide absorption in aqueous methyldiethanolamine, J. Chem. Eng. Data 34 (4) (Oct. 1989) 385–391, https://doi.org/10.1021/je00058a004.
[61] E. Álvarez, D. Gómez-Díaz, M.D. La Rubia, J.M. Navaza, Densities and viscosities of aqueous ternary mixtures of 2-(methylamino)ethanol and 2-(ethylamino) ethanol with diethanolamine, triethanolamine, N-methyldiethanolamine, or 2-Amino-1-methyl-1-propanol from 298.15 to 323.15 K, J. Chem. Eng. Data 51 (3) (May 2006) 955–962, https://doi.org/10.1021/je050463q.
[62] T.T. Teng, Y. Maham, L.G. Hepler, A.E. Mather, Viscosity of aqueous solutions of N-methyldiethanolamine and of diethanolamine, J. Chem. Eng. Data 39 (2) (Apr. 1994) 290–293, https://doi.org/10.1021/je00014a021.